Effective slip boundary conditions for arbitrary periodic surfaces: the surface mobility tensor

KEN KAMRIN[1]†, MARTIN Z. BAZANT[2] AND HOWARD A. STONE[3]

[1]School of Engineering and Applied Sciences, Harvard University, Cambridge, MA 01238, USA

[2]Departments of Chemical Engineering and Mathematics, Massachusetts Institute of Technology, Cambridge, MA 02139, USA

[3]Department of Mechanical and Aerospace Engineering, Princeton University, Princeton, NJ 08544, USA

In a variety of applications, most notably microfluidics design, slip-based boundary conditions have been sought to characterize fluid flow over patterned surfaces. We focus on laminar shear flows over surfaces with periodic height fluctuations and/or fluctuating Navier scalar slip properties. We derive a general formula for the 'effective slip', which describes equivalent fluid motion at the mean surface as depicted by the linear velocity profile that arises far from it. We show that the slip and the applied stress are related linearly through a tensorial mobility matrix, and the method of domain perturbation is then used to derive an approximate formula for the mobility law directly in terms of surface properties. The specific accuracy of the approximation is detailed, and the mobility relation is then utilized to address several questions, such as the determination of optimal surface shapes and the effect of random surface fluctuations on fluid slip.

1. Introduction

With recent progress in the study and fabrication of mirofluidic devices, new interest has arisen in determining generalized forms of hydrodynamic boundary conditions (Stone, Stroock & Ajdari 2004; Bazant & Vinogradova 2008). Advances in lithography to pattern substrates at the micrometre and nanometre length scales have raised several questions in the modelling of fluid motions over these surfaces. For example, rather than trying to solve equations of motion for the flow at the scale of the individual corrugations of the pattern, it is appropriate to consider the bulk fluid motion (on length scales much larger than the pattern wavelength) by utilizing effective boundary conditions that characterize the flow at the surface. For fluid being sheared horizontally over a textured surface, a basic aim is to derive a local boundary condition that can be applied along the smooth mean surface, which mimics the effects of the actual condition along the true surface. These effective conditions can be used in place of the no-slip condition to solve for macroscale flow without the tedium of enforcing a boundary condition on a rough boundary geometry.

† Email address for correspondence: kkamrin@seas.harvard.edu

A standard phenomenological approach for flow over a patterned surface is to assume a Navier slip boundary condition

$$\boldsymbol{u}^s = \boldsymbol{U} - \boldsymbol{u} = b\frac{\partial \boldsymbol{u}}{\partial n}, \qquad (1.1)$$

which relates the fluid velocity $\boldsymbol{u}$ at the surface, the velocity of the surface $\boldsymbol{U}$, the shear strain rate normal to the mean surface $\partial \boldsymbol{u}/\partial n$ and the scalar slip length b. This approach has been studied extensively in experiments, theoretical calculations and simulations (for recent discussion and results see Vinogradova 1999; Priezjev & Troian 2006; Bocquet & Barrat 2007; Lauga, Brenner & Stone 2007; Kunert & Harting 2008; Davis & Lauga 2009).

The above relationship avoids the possibility of flow becoming misaligned with the shearing, which has been analysed in a number of studies involving grooved surfaces (see Wang 1978, 1994, 2003; Ajdari 2002; Stroock et al. 2002a, b). Such phenomena have motivated a tensorial version of (1.1), as discussed in Stroock et al. (2002b) and Stone et al. (2004), which replaces the scalar slip length b with a rank-2 tensor $\boldsymbol{b}$ characterizing the surface anisotropy:

$$\boldsymbol{u}^s = \boldsymbol{b} \cdot (\hat{\boldsymbol{n}} \cdot \nabla \boldsymbol{u}), \qquad (1.2)$$

where $\hat{\boldsymbol{n}}$ is the unit normal (directed into the fluid). Bazant & Vinogradova (2008) proposed to express the tensorial slip condition in the convenient form of a mobility law, where the mean surface normal traction $\boldsymbol{\tau} = \hat{\boldsymbol{n}} \cdot \boldsymbol{T}$ (for $\boldsymbol{T}$ the Cauchy stress tensor) and some mobility tensor $\boldsymbol{M}$ are used instead of the velocity gradient and tensorial slip length, i.e.

$$\boldsymbol{u}^s = \boldsymbol{M} \cdot \boldsymbol{\tau}, \qquad (1.3)$$

and discussed general physical constraints on $\boldsymbol{M}$ for different types of flows and surfaces.

The work herein analyses and quantifies (1.3) for the case of Stokes flow over a broad class of weakly textured surfaces. We focus on horizontally sheared fluid over surfaces with arbitrary periodic height fluctuations, and continue the analysis later (§ 8) to surfaces that also have non-uniform hydrophobicity. To rigorously evaluate the properties of $\boldsymbol{u}^s$, our approach is to construct the flow from a family of analytical solutions to the equations of motion, which are superposed as needed to satisfy the order-by-order boundary conditions on a topographically complex surface. Section 2 defines the problem and proves the validity of (1.3) by deriving the relationship directly from the Stokes equations for a no-slip surface with arbitrary periodic height fluctuations. We then proceed in § 3 to relate the details of the surface topography to the mobility tensor. This step is considered for the case of arbitrary small periodic surface corrugations, by way of a second-order domain-level perturbation analysis employing a family of Fourier series solutions to the Stokes equations. We then use the result to derive/compute a number of consequential results: analytical results in the case of grooved surfaces (§ 5), flow optimization over surfaces of fixed heterogeneity (§ 6), and statistical results for random surfaces (§ 7). The limitations of our approximation are also deduced and quantified through an in-depth error analysis in § 4 that carries over to the appendices.

2. Problem set-up

Consider a rigid, periodic surface with height $z = H(x, y)$, with period $2L_x$ in the x direction, and period $2L_y$ in the y direction. Let $z = 0$ correspond to the bottom

of the surface, so that $H(x, y) \geqslant 0$. Above the surface is a layer of fluid (of viscosity η) satisfying the no-slip boundary condition along the surface. The fluid is sheared from above, at $z \to \infty$, by a horizontal shear traction $\boldsymbol{\tau} = (\tau_x, \tau_y, 0)$, which induces a steady flow $\boldsymbol{u}(x, y, z)$ with pressure $p(x, y, z)$. As a convention in this paper, we interchangeably represent horizontal vectors with 2 or 3 components depending on context – for example, $\boldsymbol{\tau}$ can also represent (τ_x, τ_y) in planar operations.

Let us non-dimensionalize the problem to scale η out of the analysis. Let T and $\mathscr{L}$ be arbitrary, fixed units of time and length respectively. Let the unit of stress be η/T. With these units, all system variables and fields are hereby redefined to be their dimensionless counterparts, e.g.

$$\boldsymbol{u} \to \boldsymbol{u}T/\mathscr{L}, \quad \boldsymbol{\tau} \to \boldsymbol{\tau}T/\eta, \quad p \to pT/\eta, \quad \boldsymbol{x} \to \boldsymbol{x}/\mathscr{L}, \quad H \to H/\mathscr{L}. \quad (2.1)$$

We assume that the Reynolds number is sufficiently small that the flow satisfies the three-dimensional Stokes equations. Under our non-dimensionalization, this gives

$$\nabla^2 \boldsymbol{u} = \nabla p, \quad (2.2a)$$

$$\nabla \cdot \boldsymbol{u} = 0, \quad (2.2b)$$

and the dimensionless boundary conditions are

$$\boldsymbol{u}(x, y, H(x, y)) = \boldsymbol{0}, \quad \left.\frac{\partial \boldsymbol{u}}{\partial z}\right|_{z \to \infty} = \boldsymbol{\tau}. \quad (2.3)$$

Far above the patterned surface, the flow must asymptote to a simple linear flow with uniform constant pressure. A major goal of this paper is to determine the 'effective slip' – that is, the horizontal vector $\boldsymbol{u}^s$ in the asymptotic form

$$\boldsymbol{u}(\tilde{z} \to \infty) = \boldsymbol{u}^s + \boldsymbol{\tau}\tilde{z}, \quad (2.4)$$

where $\tilde{z} \equiv z - \langle H(x, y)\rangle$ measures the distance above the space-average height of the fluctuations. By definition, a perfectly flat no-slip surface has $\boldsymbol{u}^s = \boldsymbol{0}$ regardless of $\boldsymbol{\tau}$. When the surface has height fluctuations, $\boldsymbol{u}^s$ is usually non-zero and has a direction and magnitude depending on the stress vector $\boldsymbol{\tau}$ and the surface shape.

As a consequence of the linearity of the Stokes equations, the effective slip $\boldsymbol{u}^s$ and the traction $\boldsymbol{\tau}$ must be related linearly through a 2×2 matrix relationship of the form:

$$\boldsymbol{u}^s = \boldsymbol{M} \cdot \boldsymbol{\tau}. \quad (2.5)$$

We refer to the matrix $\boldsymbol{M} = \boldsymbol{M}(H)$ as the mobility tensor for the surface $H(x, y)$ – it characterizes the dependence of the net flow properties on the direction and magnitude of the applied stress. The linearity of the relationship between $\boldsymbol{u}^s$ and $\boldsymbol{\tau}$ also means that surfaces with more than two symmetry directions must have isotropic mobility. Equation (2.5) follows from the fact that the flow solution for some traction $\boldsymbol{\tau} = (\tau_x, \tau_y)$ can be found as a superposition of the solution for a unit traction in the x direction and that of a unit traction in the y direction. Accordingly, the slip induced by $\boldsymbol{\tau}$ is a superposition of the slips from the two component cases, implying $\boldsymbol{\tau}$ and $\boldsymbol{u}^s$ must relate linearly.

3. Computing the mobility tensor

An exact formula for $\boldsymbol{M}$ in terms of $H(x, y)$ seems very complicated to obtain, and unlikely to have a tractable form. In the following sections, we derive an approximate

formula for the **M** tensor in the case of small height fluctuations, i.e.

$$H(x, y) = \epsilon h(x, y) \tag{3.1}$$

for ϵ some small dimensionless number.

It is difficult to ascribe a single physical description to ϵ at the outset, since there are an infinite number of possible size scales that could be extracted from an arbitrary periodic surface. To approach this question systematically, our strategy is to obtain an approximate solution for **M** using domain perturbation theory treating ϵ as a small parameter, and then perform a separate analysis to determine the dependence of the error on $h(x, y)$. From these results, we then surmise a single property of the surface that must be small for the approximation to be accurate.

We now summarize the major result of this paper. Let $\hat{h}(m, n)$ compose the set of Fourier coefficients corresponding to $h(x, y)$,

$$h(x, y) = \sum_{m,n} \hat{h}(m, n) e^{i(k_m x + k_n y)}, \tag{3.2}$$

where $k_m = m\pi/L_x$ and $k_n = n\pi/L_y$ are corresponding wavenumbers. Then the effective slip velocity obeys

$$\boldsymbol{u}^s = -\epsilon^2 \tilde{\boldsymbol{M}}(h) \cdot \boldsymbol{\tau} + O(\epsilon^3), \tag{3.3}$$

where the function $\tilde{\boldsymbol{M}}(h)$ is defined by

$$\tilde{\boldsymbol{M}}(h) = \begin{pmatrix} \displaystyle\sum_{(m,n)\neq 0} \frac{2k_m^2 + k_n^2}{\sqrt{k_m^2 + k_n^2}} |\hat{h}(m, n)|^2 & \displaystyle\sum_{(m,n)\neq 0} \frac{k_m k_n}{\sqrt{k_m^2 + k_n^2}} |\hat{h}(m, n)|^2 \\ \displaystyle\sum_{(m,n)\neq 0} \frac{k_m k_n}{\sqrt{k_m^2 + k_n^2}} |\hat{h}(m, n)|^2 & \displaystyle\sum_{(m,n)\neq 0} \frac{k_m^2 + 2k_n^2}{\sqrt{k_m^2 + k_n^2}} |\hat{h}(m, n)|^2 \end{pmatrix}. \tag{3.4}$$

First, observe that the mobility is an $O(\epsilon^2)$ effect for height fluctuations of size $O(\epsilon)$. A second-order leading term was also observed in Tuck & Kouzoubov (1995) and Stroock *et al.* (2002*b*) for the effective slip of shear flow over a shallow sinusoidal wall and slip in pressure-driven Poiseuille flow between sinusoidal walls, respectively. Furthermore, the leading-order mobility matrix is symmetric regardless of $h(x, y)$ (within the broad range of validity of the analysis, quantified below). This result was suggested, though not proved, in Bazant & Vinogradova (2008), where the notion of symmetric mobility was supported by a statistical diffusion argument and treated as an example of the commonly used Onsager–Casimir relations for near-equilibrium linear response. The symmetry of $\tilde{\boldsymbol{M}}$ requires that its eigenvectors are orthogonal, and likewise a general surface H should have two orthogonal directions along which the shear stress and slip direction align. If stress is applied in a different direction, the apparent slip can have lateral components that transport fluid transverse to the direction of the stress traction, as in Stroock *et al.* (2002*b*) and Stone *et al.* (2004).

It is also important to note that with the definitions used here, (3.3) and (3.4) give a negative-definite mobility. That is, the effective slip should point away from the traction vector (see figure 1*b*), which reflects the notion that surface fluctuations cause flow resistance compared to a flat surface of the same mean height. This outcome can also be seen as directly related to our choice of placing the origin for $\tilde{z}$ at the mean height of the pattern. In studies such as Wang (2003), the origin is placed at the peak of the height fluctuations, which redefines the slip vector in a way that ensures $\boldsymbol{\tau} \cdot \boldsymbol{u}^s \geqslant 0$,
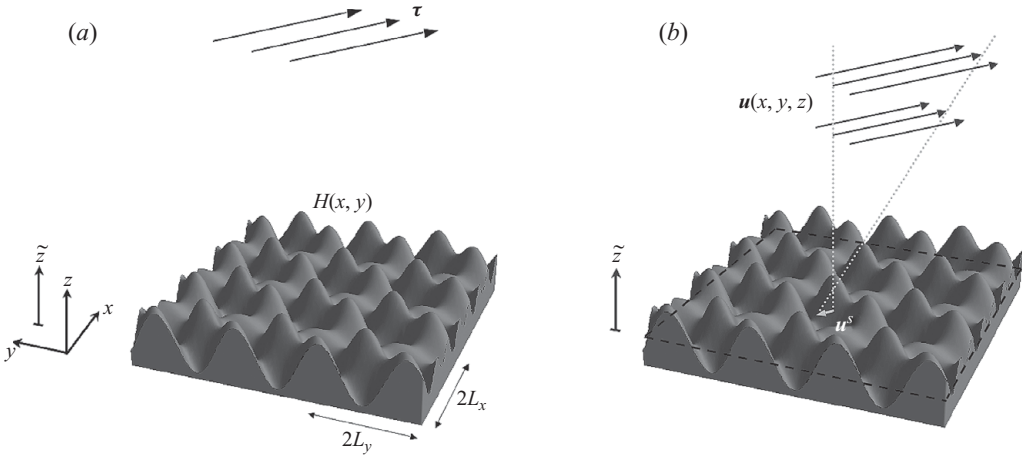
FIGURE 1. (*a*) Set-up for the problem. A fluid is horizontally sheared with stress $\boldsymbol{\tau}$ at a height of $\tilde{z} = \infty$ above a surface with arbitrary periodic height fluctuations $H(x, y)$. (*b*) The induced flow profile becomes horizontal and linear in $\tilde{z}$ at large heights, but is more complicated closer to the surface. Our interest is to determine the effective slip $\boldsymbol{u}^s$, pictured above, which corresponds to the extra velocity one would obtain when extrapolating the linear portion down to the mean surface height $\tilde{z} = 0$.

and equivalently redefines the mobility tensor to be positive definite. Positive mobility is desirable from an intuitive standpoint because it more closely represents an object slipping on a dissipative, 'passive surface' (Bazant & Vinogradova 2008). However, for our purposes, we find it computationally easier to perform our analyses with the mean surface height selected as the origin. Other effective slip studies such as Stroock *et al.* (2002*b*) and Panzer, Liu & Einzel (1992) also set the origin at the surface mean.

The mobility relation can be used as a general boundary condition for surfaces whose corrugations are small compared to the typical length scale of the macroscopic environment, so that the conditions resemble figure 1 near the wall. For example, Panzer *et al.* (1992) evaluates pressure-driven viscous flow between two sinusoidal walls separated a large distance compared to the wavelength. To second order in the amplitude to wavelength ratio, their result for the effective slip length matches the solution one would obtain by replacing the walls with flat planes and applying (3.3) as the boundary condition.

The remainder of this section details the derivation of (3.3) and (3.4).

3.1. *Perturbation expansion*

Our approach utilizes the method of domain perturbations (see Hinch 1991), which has been useful in a variety of past slip studies (Wang 1978, 2004; Luchini, Manzo & Pozzi 1991; Panzer *et al.* 1992; Miksis & Davis 1994; Tuck & Kouzoubov 1995; Zhou, Martinuzzi & Straatman 1995). Here, we compute the three-dimensional flow profile up to second order, as is necessary to reveal the tensorial properties of the effective slip.

To begin, we let the velocity and pressure fields be represented by the perturbation series

$$(\boldsymbol{u}, p) = (\boldsymbol{u}_0, p_0) + \epsilon(\boldsymbol{u}_1, p_1) + \epsilon^2(\boldsymbol{u}_2, p_2) + O(\epsilon^3). \tag{3.5}$$

Using the method of domain perturbations, the expression of the boundary condition along the periodic surface is expanded in a Taylor series about $z = 0$:

$$\boldsymbol{u}(x, y, \epsilon h(x, y)) = \boldsymbol{0} = \boldsymbol{u}_0(x, y, 0) + \epsilon h(x, y) \left.\frac{\partial \boldsymbol{u}_0}{\partial z}\right|_{z=0} + \frac{(\epsilon h(x, y))^2}{2} \left.\frac{\partial^2 \boldsymbol{u}_0}{\partial z^2}\right|_{z=0}$$

$$+ \epsilon \left(\boldsymbol{u}_1(x, y, 0) + \epsilon h(x, y) \left.\frac{\partial \boldsymbol{u}_1}{\partial z}\right|_{z=0}\right) + \epsilon^2 \boldsymbol{u}_2(x, y, 0) + O(\epsilon^3).$$

This expression is equivalent to three separate boundary conditions for the first three orders:

$$\boldsymbol{u}_0(x, y, 0) = \boldsymbol{0}, \tag{3.6a}$$

$$\boldsymbol{u}_1(x, y, 0) = -h(x, y) \left.\frac{\partial \boldsymbol{u}_0}{\partial z}\right|_{z=0}, \tag{3.6b}$$

$$\boldsymbol{u}_2(x, y, 0) = -h(x, y) \left.\frac{\partial \boldsymbol{u}_1}{\partial z}\right|_{z=0} - \frac{h(x, y)^2}{2} \left.\frac{\partial^2 \boldsymbol{u}_0}{\partial z^2}\right|_{z=0}. \tag{3.6c}$$

The traction condition at $z \to \infty$ is first-order in magnitude, which implies the following three boundary conditions:

$$\left.\frac{\partial \boldsymbol{u}_0}{\partial z}\right|_{z=\infty} = \boldsymbol{\tau}, \quad \left.\frac{\partial \boldsymbol{u}_1}{\partial z}\right|_{z=\infty} = \boldsymbol{0}, \quad \left.\frac{\partial \boldsymbol{u}_2}{\partial z}\right|_{z=\infty} = \boldsymbol{0}. \tag{3.7}$$

3.2. Solving for horizontally periodic Stokes flow

By inspection, we find that the zeroth-order solution is simple shear:

$$\boldsymbol{u}_0(x, y, z) = \boldsymbol{\tau} z, \quad p_0(x, y, z) = K_0, \tag{3.8}$$

where K_0 is a constant. To compute each of the higher-order terms, we need an analytic general solution to the Stokes equations that satisfies the $z \to \infty$ boundary condition. From such a general solution, we can fit the more complicated $z = 0$ boundary conditions. Since the surface is periodic, any flow solution must exhibit the same periodicity. Hence,

$$\boldsymbol{u}(x, y, z) = \sum_{m,n} \boldsymbol{a}(m, n, z) e^{i(k_m x + k_n y)}, \quad p(x, y, z) = \sum_{m,n} b(m, n, z) e^{i(k_m x + k_n y)}. \tag{3.9}$$

Substituting these forms into the Stokes equations, a general solution for $\boldsymbol{a}$ and b can be found (see Appendix A), which ultimately depends on three sets of undetermined coefficients. Whenever m and n are non-zero, $\boldsymbol{a}$ and b both decay exponentially in z as expected, which guarantees satisfaction of the upper boundary condition.

3.3. First-order term

To solve for the first-order flow, the undetermined coefficients are solved term-by-term by enforcing the bottom boundary condition (3.6b), which now reads

$$\boldsymbol{u}_1(x, y, 0) = -h(x, y)\boldsymbol{\tau}. \tag{3.10}$$

The result is

$$u_1(x, y, z) = -\hat{h}(0,0)\tau_x + \sum_{(m,n)\neq 0} \hat{h}(m,n)e^{-\sqrt{k_m^2+k_n^2}\,z}\left(\frac{k_m\tau_x + k_n\tau_y}{\sqrt{k_m^2+k_n^2}}k_m z - \tau_x\right)e^{i(k_m x + k_n y)}, \tag{3.11}$$

$$v_1(x, y, z) = -\hat{h}(0,0)\tau_y + \sum_{(m,n)\neq 0} \hat{h}(m,n)e^{-\sqrt{k_m^2+k_n^2}\,z}\left(\frac{k_m\tau_x + k_n\tau_y}{\sqrt{k_m^2+k_n^2}}k_n z - \tau_y\right)e^{i(k_m x + k_n y)}, \tag{3.12}$$

$$w_1(x, y, z) = \sum_{(m,n)\neq 0} \hat{h}(m,n)\mathrm{i}e^{-\sqrt{k_m^2+k_n^2}\,z}(k_m\tau_x + k_n\tau_y)z\,e^{i(k_m x + k_n y)}, \tag{3.13}$$

$$p_1(x, y, z) = K_1 + \sum_{(m,n)\neq 0} \hat{h}(m,n)2\mathrm{i}e^{-\sqrt{k_m^2+k_n^2}\,z}(k_m\tau_x + k_n\tau_y)e^{i(k_m x + k_n y)}, \tag{3.14}$$

where $\boldsymbol{u}_1 = (u_1, v_1, w_1)$ and K_1 is an arbitrary constant. The constant terms in the u_1 and v_1 expansions grow proportionally to the average surface height $\hat{h}(0,0)$, and provide a first-order isotropic slip contribution, as all other terms decay exponentially as $z \to \infty$.

3.4. *Second-order term*

To determine the second-order solution, we take the general solution from Appendix A and enforce the $z = 0$ boundary condition, which now reads

$$\boldsymbol{u}_2(x, y, 0) = -h(x, y)\left.\frac{\partial \boldsymbol{u}_1}{\partial z}\right|_{z=0}, \tag{3.15}$$

where

$$\left.\frac{\partial u_1}{\partial z}\right|_{z=0} = \sum_{(m,n)\neq 0} \frac{2k_m^2\tau_x + k_n^2\tau_x + k_m k_n\tau_y}{\sqrt{k_m^2+k_n^2}}\hat{h}(m,n)e^{i(k_m x + k_n y)}, \tag{3.16}$$

$$\left.\frac{\partial v_1}{\partial z}\right|_{z=0} = \sum_{(m,n)\neq 0} \frac{2k_n^2\tau_y + k_m^2\tau_y + k_m k_n\tau_x}{\sqrt{k_m^2+k_n^2}}\hat{h}(m,n)e^{i(k_m x + k_n y)}, \tag{3.17}$$

$$\left.\frac{\partial w_1}{\partial z}\right|_{z=0} = \sum_{(m,n)\neq 0} \mathrm{i}(k_m\tau_x + k_n\tau_y)\hat{h}(m,n)e^{i(k_m x + k_n y)}, \tag{3.18}$$

as follows from (3.11), (3.12) and (3.13).

Since we are stopping the perturbation analysis beyond $O(\epsilon^2)$, there is no need to compute the full solution for $\boldsymbol{u}_2$ – one need only determine the constant term in its Fourier series solution, (3.9). This term will be the only one that does not vanish as $z \to \infty$, and represents the effective slip. A full solution to $\boldsymbol{u}_2$ is necessary later and detailed in Appendix C. Denoting $\langle f(x, y)\rangle$ as the horizontal spatial average of f, note that the constant term in the Fourier expansion of $\boldsymbol{u}_2(x, y, z)$ is necessarily equal to $\langle\boldsymbol{u}_2\rangle$ at any fixed z, since all other terms average to zero over $[-L_x, L_x] \times [-L_y, L_y]$. Hence,

$$\boldsymbol{u}_2^s = \langle\boldsymbol{u}_2(x, y, 0)\rangle = -\left\langle h(x, y)\left.\frac{\partial\boldsymbol{u}_1}{\partial z}\right|_{z=0}\right\rangle. \tag{3.19}$$

Since the term on the right-hand side is the average of the product of two periodic functions of equal periodicity, we obtain $\boldsymbol{u}_2^s$ from the product of the two Fourier

expansions. For any coefficients $\alpha(m, n)$, recall the general rule

$$\left\langle h(x, y) \sum_{m,n} \alpha(m, n)\hat{h}(m, n)e^{i(k_m x + k_n y)} \right\rangle = \sum_{m,n} \alpha(m, n)\hat{h}(m, n)\hat{h}(-m, -n)$$

$$= \sum_{m,n} \alpha(m, n)|\hat{h}(m, n)|^2. \quad (3.20)$$

Applying this rule to the given boundary conditions, we uncover the tensor $\tilde{\boldsymbol{M}}(h)$ from (3.4), giving

$$\boldsymbol{u}_2^s = -\tilde{\boldsymbol{M}}(h) \cdot \boldsymbol{\tau}. \quad (3.21)$$

Combining the constant terms from the first- and second-order flows with the zeroth-order shear flow, and then switching to the variable $\tilde{z}$, we obtain the limiting behaviour

$$\boldsymbol{u}(\tilde{z} \to \infty) = \boldsymbol{\tau}\tilde{z} - \epsilon^2 \tilde{\boldsymbol{M}}(h) \cdot \boldsymbol{\tau} + O(\epsilon^3), \quad (3.22)$$

and the slip formula (3.3) immediately follows.

4. Error analysis

4.1. *The need to compute error bounds*

The significance of the slip approximation (3.3) is tied directly to the error of truncating the perturbation expansion at second order. It is of critical importance that we quantify this error to correctly interpret the mobility matrix approximation $\boldsymbol{M}(\epsilon h) \approx -\epsilon^2 \tilde{\boldsymbol{M}}(h)$.

For example, consider a surface of shallow, square grooves – that is, $H(x, y) = \epsilon h(x, y)$, where

$$h(x, y) = \begin{cases} 1 & \text{if } 2k < x \leqslant 2k + 1 \text{ for integer } k, \\ 0 & \text{if } 2k + 1 < x \leqslant 2k + 2 \text{ for integer } k. \end{cases} \quad (4.1)$$

For this surface, the sums in the mobility approximation (3.4) diverge, giving infinite values for $\tilde{M}_{11}$ and $\tilde{M}_{22}$. This prediction is clearly erroneous, as it suggests an infinite slip velocity (regardless of the choice of $\epsilon > 0$), contradicting known results in Wang (2003) and basic intuition.

In view of (3.3), the error term must be expressible as $\epsilon^3 C(h, \boldsymbol{\tau})$ for some unknown function C. As just demonstrated, certain surfaces h cause $C(h, \boldsymbol{\tau})$ to become large or infinite, which overwhelms the fact that the prefactor is ϵ^3 small. Hence, in the upcoming subsection, we bound $|C(h, \boldsymbol{\tau})|$ by some known form $|\boldsymbol{\tau}|\mathrm{Err}(h)$, so that

$$|\boldsymbol{u}^s - (-\epsilon^2 \tilde{\boldsymbol{M}}(h) \cdot \boldsymbol{\tau})| \leqslant \epsilon^3 |\boldsymbol{\tau}| \, \mathrm{Err}(h). \quad (4.2)$$

Once the function Err is determined, we can affirm that the mobility matrix approximation $\boldsymbol{M} \approx -\epsilon^2 \tilde{\boldsymbol{M}}$ is valid for any surface where the error bound is small compared to the approximate slip, i.e.

$$\text{relative error bound} = \frac{\epsilon^3 \mathrm{Err}(h)|\boldsymbol{\tau}|}{|-\epsilon^2 \tilde{\boldsymbol{M}}(h) \cdot \boldsymbol{\tau}|} \approx \frac{\epsilon^3 \mathrm{Err}(h)}{\epsilon^2 |\tilde{\boldsymbol{M}}(h)|} \ll 1, \quad (4.3)$$

where $|\cdot|$ applied to matrices implies the Euclidean norm. This relation gives an *a priori* method for ruling out surface shapes that do not comply with our approximation.

Below, we show that (4.3) can also be used to determine an ideal definition of ϵ in terms of properties of the surface. Up to this point, we have described ϵ merely as a

'small dimensionless number', and $h(x, y)$ is defined as $H(x, y)/\epsilon$. A specific formula for ϵ as a function of the surface $H(x, y)$ is physically desirable, wherein the size of ϵ immediately relates to the accuracy of the approximation.

4.2. *Bounding the approximation error*

The error of the slip approximation arises solely from error in fitting the boundary condition $\boldsymbol{u}(x, y, \epsilon h(x, y)) = \boldsymbol{0}$, since our method is guaranteed to satisfy the Stokes equations in the bulk. Appendix B constructs a bound on this error, which leads to the following bound on the error of the second-order slip approximation:

$$|\boldsymbol{u}^s - (-\epsilon^2 \tilde{\boldsymbol{M}}(h) \cdot \boldsymbol{\tau})| \leqslant \epsilon^3 \kappa h_M |\boldsymbol{\tau}| \big(h_M \, |\boldsymbol{\nabla}\boldsymbol{\nabla}h|_M + |\boldsymbol{\nabla}h|_M^2 \big), \tag{4.4}$$

where we use the subscript 'M' to denote a function's maximum value over all x and y. The constant κ is dimensionless and independent of $\boldsymbol{\tau}$ and the surface shape; a first calculation gives $\kappa < 55$. Based on the analysis in Appendices B and C, we speculate that it is not possible to bound the error in a general fashion using fewer than the first two derivatives of h. While this decrees a qualitative level of tightness, it is clear from the appendices that quantitatively tighter bounds could be written using non-local norms and surface integrals. We prefer the above, as it is expressible using basic quantities. Recent work on bounding the error of Reynolds' lubrication approximation for thin-channel Stokes flows (Wilkening 2009) has found some similar dependences on the norms of the derivatives of the surface.

Equation (4.4) reveals that the error is unbounded for any surface where $|\boldsymbol{\nabla}\boldsymbol{\nabla}h|_M$ or $|\boldsymbol{\nabla}h|_M \to \infty$. Hence, the approximation $\boldsymbol{M}(\epsilon h) \approx -\epsilon^2 \tilde{\boldsymbol{M}}(h)$ should not be used for surfaces with corners or vertical slopes. This point, which may not surprise those familiar with applications of domain perturbation, provides an explanation for why the previous square grooves example failed. Note that the error does not depend at all on the higher-order derivatives of h (order $\geqslant 3$), and as such the approximation can be accurate even if these derivatives are discontinuous.

Equation (4.4) also implies a formula for the function Err that was sought after in (4.2):

$$\text{Err}(h) = \kappa h_M \big(h_M \, |\boldsymbol{\nabla}\boldsymbol{\nabla}h|_M + |\boldsymbol{\nabla}h|_M^2 \big). \tag{4.5}$$

Observing (4.5) and (3.4), we note that the relative error bound (4.3) can be expressed solely in terms of the actual surface $H(x, y)$, and completely independent of ϵ, since all powers of ϵ can be brought into the arguments of the functions $\tilde{\boldsymbol{M}}$ and Err, and eliminated by using $H = \epsilon h$:

$$\text{relative error bound} = \frac{\epsilon^3 \text{Err}(h)}{\epsilon^2 |\tilde{\boldsymbol{M}}(h)|} = \frac{\text{Err}(H)}{|\tilde{\boldsymbol{M}}(H)|}. \tag{4.6}$$

This last expression is a dimensionless ratio determined entirely by the given surface $H(x, y)$. While it may not be simple to interpret physically for a general surface, its direct connection to the error suggests an ideal formula for choosing ϵ given $H(x, y)$ would be

$$\epsilon_{ideal} \equiv \frac{\text{Err}(H)}{|\tilde{\boldsymbol{M}}(H)|}. \tag{4.7}$$

The relative approximation error can never exceed ϵ_{ideal}, and hence all surfaces with a small value for ϵ_{ideal} are well described by the mobility formula (3.4). If we let $\epsilon = \epsilon_{ideal}$ in (4.2), and consequently $h(x, y) = H(x, y)/\epsilon_{ideal}$, then the slip relation can be rewritten as

$$\big|\boldsymbol{u}^s - \big(-\epsilon_{ideal}^2 \tilde{\boldsymbol{M}}(h) \cdot \boldsymbol{\tau}\big)\big| \leqslant \epsilon_{ideal}^3 \, |\tilde{\boldsymbol{M}}(h)| \, |\boldsymbol{\tau}|. \tag{4.8}$$

As a simple demonstration, consider the surface $H(x, y) = a \sin(x/b)$ for constants a and b. In agreement with Tuck & Kouzoubov (1995), we find $M_{11} \propto -a^2/b$, and we similarly expect the approximation to improve as a/b decreases to zero. This is confirmed by (4.7), giving $\epsilon_{ideal} = (8\kappa/\sqrt{5})(a/b)$ as the relevant small quantity, proportional to a/b as expected. As a/b increases beyond the small limit, the approximation indeed fails; Hocking (1976) shows that the true mobility approaches a constant as b increases at fixed a. The approach to a constant slip length with increasing groove depth is not surprising and occurs as well for other surface geometries (Bechert & Bartenwerfer 1989; Luchini et al. 1991; Wang 2003).

The limitations of our approach highlight the importance of past studies that compute the effective slip over certain families of surfaces containing corners and/or vertical walls. Sarkar & Prosperetti (1996) have evaluated shear flow over surfaces embossed with compact bumps, which make sharp corners where attached to the adjacent surface. Wang (1994, 2003) consider, respectively, flows over finned surfaces and surfaces with parallel rectangular grooves, for which infinite curvature and slope both occur. Higdon (1985) describes a numerical procedure for computing two-dimensional shear flow over any type of curved/kinked surface, which could then be used to extract the effective mobility.

5. Mobility over surfaces varying in only one direction

Our main result above (3.4) is useful in revealing general properties of the effective slip and, within the error bounds, to allow its computation for an arbitrary surface. However, the various series for the elements of $\tilde{\boldsymbol{M}}$ can be cumbersome to evaluate. Of course, it is easy to evaluate them for surfaces with simple sinusoidal perturbations, which have Fourier series truncated after a small number of terms, but this offers little analytical insight into the dependence of the mobility tensor on the shape of the surface. To see this dependence more clearly, this section focuses on a simpler family of surfaces.

Observing (3.4), we note that the formula reduces significantly for the class of surfaces varying in only one direction. Letting the variation direction be x, these surfaces appear as parallel groove patterns with shape $h(x)$ and mobility

$$\boldsymbol{M} \approx -\epsilon^2 \tilde{\boldsymbol{M}}(h) = -\epsilon^2 \beta \begin{pmatrix} 2 & 0 \\ 0 & 1 \end{pmatrix} \qquad \text{for } \beta = 2 \sum_{m=1}^{\infty} k_m |\hat{h}(m)|^2. \tag{5.1}$$

This result is consistent with the findings of Luchini et al. (1991) – exploiting y-invariance, they performed separate two-dimensional computations for flow along and transverse to shallow grooves, and found series representations agreeing with (5.1). The above formula implies the slip length (which measures distance from the mean surface height to the equivalent no-slip plane) is generally twice as large for perpendicular versus parallel shearing. For anisotropic Stokes flow, factors of two like this are not surprising – it is reminiscent of similar results for striped pipes (Lauga & Stone 2003) and the classical result that a rod sediments twice as fast in creeping flow if aligned vertically, rather than horizontally (Batchelor 1970).

Let us evaluate $\boldsymbol{M}$ in closed form for a non-trivial subset of grooved surfaces, whose Fourier series have an infinite number of terms, and vary continuously in shape from sinusoidal to sharply peaked. Consider surface shapes $h(x)$ of the type

$$h(x) = \frac{\phi(x) - \phi_{min}}{\phi_{max} - \phi_{min}}, \qquad \phi(x) = \frac{1}{1 + a^2 + 2a \cos x} \tag{5.2}$$
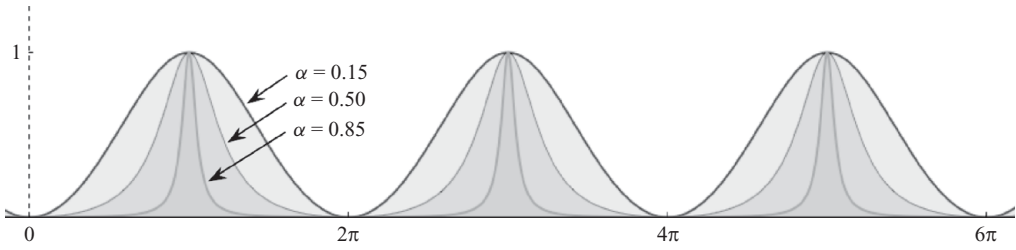
FIGURE 2. The surface shape $h(x)$, defined in (5.2), under different values of the parameter a.

with unit of length $\mathcal{L} = L_x/\pi$, so that $k_m = m$. Regardless of the parameter $0 < a < 1$, $h(x)$ has a maximum of 1, and a minimum of 0. As shown in figure 2, a controls the shape of the surface. For $a \ll 1$, the surface height is a small perturbation from a single-mode sinusoid. As $a \to 1$, the surface develops wide, deep valleys around the minimum height at $x = 2n\pi$ separated by tall, narrow peaks at $x = (2n+1)\pi$.

The Fourier coefficients of $h(x)$ can be obtained directly from those of $\phi(x)$. Set $z = e^{ix}$ to express ϕ as a rational function $f(z)$, separate into partial fractions, and expand in geometric series (since $|az| = |a/z| < 1$) to obtain the Laurent series of $f(z)$, which equals the desired Fourier series on the unit circle. This ultimately gives

$$\hat{h}(m \neq 0) = \frac{a^2 - 1}{4a}(-a)^{|m|}.$$ (5.3)

By (5.1),

$$\beta = 2 \sum_{m=1}^{\infty} \left(\frac{a^2 - 1}{4a}\right)^2 m(-a)^{2m} = \left(\frac{a^2 - 1}{4a}\right)^2 a \frac{\mathrm{d}}{\mathrm{d}a} \sum_{m=0}^{\infty} a^{2m} = \frac{1}{8}.$$ (5.4)

We observe that for this specific family of surfaces, β does not vary with a. However, the observed slip properties will vary, since the average surface height, at which the slip calculation applies, does change with a. We use (5.1) to compute a second-order approximation of the equivalent no-slip plane (denoted z^{NS}, i.e. the height of the plane having zero mean velocity) corresponding to each a under both parallel and transverse shear. The mean surface height obeys $\epsilon\langle h \rangle = \epsilon(1-a)/2$, and consequently, for any ϵ and unit applied shear stress, we have, to second order,

$$z_{\parallel}^{NS} \approx \epsilon \frac{1-a}{2} + \frac{\epsilon^2}{8},$$ (5.5a)

$$z_{\perp}^{NS} \approx \epsilon \frac{1-a}{2} + \frac{\epsilon^2}{4}.$$ (5.5b)

This qualitatively states that as a increases, the effective no-slip plane descends (regardless of the shear direction). In physical terms, the fluid content in the groove pattern increases with a, which increases the lubrication of the surface. The directionality of the surface comes in at second order, where the added flow resistance of shearing transverse to the grooves is apparent.

As a increases, it is important to keep in mind the accuracy of the approximation. The second derivative of h and the square of the first derivative both diverge as $(1-a)^{-2}$ as $a \to 1$. Hence, (4.4) implies the error bound on z^{NS} must also diverge as $a \to 1$,

$$\Delta z_{\parallel}^{NS}, \ \Delta z_{\perp}^{NS} \leqslant O(\epsilon^3(1-a)^{-2}).$$ (5.6)
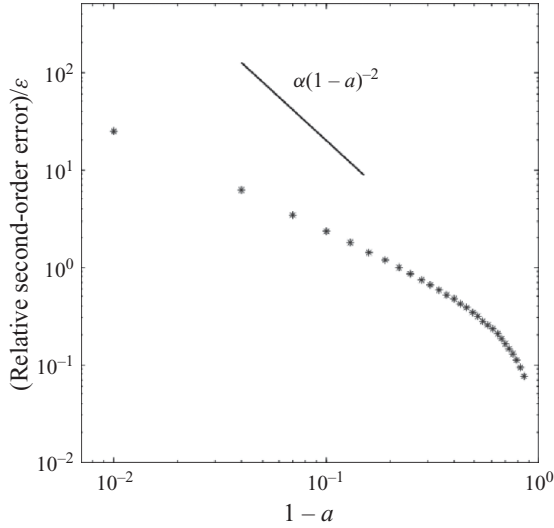
FIGURE 3. The true error of the second-order approximation for $z_\parallel^{NS}$ relative to the size of the second-order correction (i.e. $\epsilon^2/8$) versus the value of a. The rate of divergence near $a = 1$ is notably lower than our conservative error bound $\propto (1-a)^{-2}$.

Such a bound is useful for detecting qualitative behaviour of the accuracy, however, as is common with asymptotic methods like domain perturbation, the actual error is commonly well under the bound.

To test this, we compute a near-exact flow solution for parallel shear over the family of surfaces (5.2). Since the velocity is always parallel to the grooves, the problem reduces to solving the Laplace equation for the in-line component $v(x, z)$ under the boundary conditions $v_z(z = \infty) = \tau \equiv 1$ and $v(x, \epsilon h(x)) = 0$. This can be solved as a superposition of separable solutions

$$v(x, z) = z + \sum_{m=0}^{\infty} A_m \cos(mx) \exp(-mz), \tag{5.7}$$

where the A_m are chosen to satisfy the no-slip boundary condition. To compute a numerical solution, we solve for the first 1000 terms A_m by enforcing the boundary condition on 1000 equally spaced x values from 0 to π.

Flows are solved using a values ranging from 0.15 to 0.99 in increments of 0.03. For each a, the flow is computed using seven ϵ values decreasing from 10^{-1} to 10^{-4} logarithmically. Our goal is to determine how accurate (5.5a) is compared to the finest term of the approximation, the second-order correction $\epsilon^2/8$. Hence, for each a and ϵ pair, we compute the relative second-order error – the difference between the near-exact numerical solution for $z_\parallel^{NS}$ and the second-order approximation (5.5a), scaled by the size of the second-order correction term $\epsilon^2/8$. As suggested by the error bound (5.6), the relative second-order error comes out as being proportional to ϵ and diverges to ∞ as $a \to 1$. But, as a bound, we are not surprised to see it exceeds the true error as $a \to 1$. Even so, it is likely that the concessions we made to simplify the formula for the bound contribute to the slope difference evident in figure 3. From the plot, we see that if $\epsilon = 0.1$, for example, then as long as a is less than about 0.8, the prediction for the no-slip plane is accurate to within one-tenth of the size of the second-order term.

6. Optimizing slip properties

With a direct approximation for the mobility matrix and bounds for the error, we now attempt to determine which surface shapes minimize/maximize the effective slip. Problems of this type, relating to flow optimization with rigid interfaces, have been looked at primarily in three dimensions, through elegant analyses of optimally porous structures for fluid permeability (see Jung & Torquato 2005). Here we study essentially a reduced dimensional problem of optimizing the effective planar slip with respect to a rigid boundary. Similar questions regarding optimal wall geometry have also been analysed in various limits of channel flow (Wang 2004; Feuillebois, Bazant & Vinogradova 2009).

Let us define

$$\text{forward mobility} = \frac{u^s \cdot (\tau/|\tau|)}{|\tau|} \approx -\frac{\epsilon^2}{|\tau|^2}(\tau \cdot \tilde{M}(h) \cdot \tau), \qquad (6.1)$$

which measures how much slip occurs in the direction of τ per unit shear stress. As is evident from (3.4), the most forward mobility occurs when the surface is perfectly flat: if $h(x, y) = \text{const.}$, then $\tilde{M} = 0$ and $u^s = 0$ (as expected from a flat no-slip surface). For all other surfaces, $\tilde{M}$ is necessarily positive definite and the forward mobility must be negative. In simple terms, fluctuating surfaces always resist flow more than flat surfaces. However, it should be duly pointed out that in other geometries, surface fluctuations can reduce flow resistance. For instance, in Poiseuille flow between two bumpy sheets, Wang (2004) showed that the net flow can exceed the value for flat surfaces when the sheet separation is small (which places the problem outside our current scope).

We now investigate the question of how to maximize/minimize the mobility given that $h(x, y)$ must have some fixed level of heterogeneity. We quantify the heterogeneity through the variance of $h(x, y)$:

$$\text{Var}(h) = \langle (h(x, y) - \langle h(x, y) \rangle)^2 \rangle = \sum_{(m,n) \neq 0} |\hat{h}(m, n)|^2.$$

6.1. *Maximal forward mobility*

Suppose ϵ is fixed, $L_x = L_y \equiv L$, and $h(x, y)$ is constrained to have a fixed variance σ^2. We now derive the surface shape $h(x, y)$ that maximizes the mobility. This is essentially a Lagrange multiplier problem where the unknowns are the coefficients $|\hat{h}(m, n)|$. Without loss of generality, presume τ is aligned with the x direction. Then our goal is to minimize

$$\hat{x} \cdot \tilde{M} \cdot \hat{x} = \tilde{M}_{11} = \sum_{(m,n) \neq 0} \frac{2k_m^2 + k_n^2}{\sqrt{k_m^2 + k_n^2}} |\hat{h}(m, n)|^2$$

subject to the constraint

$$\text{Var}(h) = \sum_{(m,n) \neq 0} |\hat{h}(m, n)|^2 = \sigma^2. \qquad (6.2)$$

The critical points occur only for

$$\nabla_{|\hat{h}(m,n)|} \tilde{M}_{11}(h) = \lambda \nabla_{|\hat{h}(m,n)|} \text{Var}(h)$$

for Lagrange multiplier λ. Evaluating this form gives

$$2\frac{2k_m^2 + k_n^2}{\sqrt{k_m^2 + k_n^2}}|\hat{h}(m, n)| = 2\lambda|\hat{h}(m, n)| \quad \text{for all} \quad (m, n) \neq \mathbf{0}. \tag{6.3}$$

Hence, any surface constituting a critical point of the Lagrange multiplier problem can only contain modes with the same value of $(2k_m^2 + k_n^2)/\sqrt{k_m^2 + k_n^2}$. Any critical point containing a certain mode $e^{i(k_\alpha x + k_\beta y)}$ must, by (6.2) and (3.4), have

$$\tilde{M}_{11} = \frac{2k_\alpha^2 + k_\beta^2}{\sqrt{k_\alpha^2 + k_\beta^2}}\sigma^2. \tag{6.4}$$

Of these critical $\tilde{M}_{11}$ values, the minimum value is $\tilde{M}_{11} = \pi\sigma^2/L$, which occurs only for $(\alpha, \beta) = (0, \pm 1)$. Together with the fact that $\hat{h}(m, n) = \hat{h}(-m, -n)^*$, we obtain

$$\hat{h}(0, 1) = \frac{\sigma}{\sqrt{2}}e^{i\phi}, \quad \hat{h}(0, -1) = \frac{\sigma}{\sqrt{2}}e^{-i\phi} \quad \text{and} \quad \hat{h}(m \neq 0, n \neq \pm 1) = 0$$

for some constant phase ϕ. The minimizing surface given our constraints is then

$$h(x, y) = \frac{\sigma}{\sqrt{2}}e^{i\phi}e^{i\pi y/L} + \frac{\sigma}{\sqrt{2}}e^{-i\phi}e^{-i\pi y/L} = \sigma\sqrt{2}\,\cos\left(\frac{\pi y}{L} + \phi\right). \tag{6.5}$$

Thus, at fixed variance, the least resistance to forward flow occurs when the surface is a single-mode sinusoid and the fluid is pushed in the direction along the grooves. Moreover, the ideal wavelength of the surface is the longest one allowable for the given periodicity.

6.2. *Minimal forward mobility*

Before determining the surface shape with the least forward mobility, an important caveat must be included: to wit, we constrict the allowable bandwidth of the surface. For some positive K, consider only scaled surfaces of the form

$$h(x, y) = \sum_{\left\{m, n:\, 0 < \sqrt{k_m^2 + k_n^2} < K\right\}} \hat{h}(m, n)e^{i(k_m x + k_n y)}. \tag{6.6}$$

Capping the bandwidth is the simplest way to avoid surfaces that violate the second-order accuracy of the perturbation expansion. Naive observation of (6.4) would suggest that minimal mobility occurs as $\alpha, \beta \to \infty$, as this maximizes the critical values of $\tilde{M}_{11}$. But, in view of the error bound (4.4), we see that such a solution violates the accuracy requirements, as it corresponds to a surface with infinite frequency and hence unbounded slope and curvature. By considering only surfaces of a finite bandwidth, we guarantee there exists a single, fixed ϵ so that all critical points of the Lagrange multiplier problem correspond to sufficiently accurate solutions.

This being said, we reduce to the problem of minimizing the forward mobility over the set of surface shapes h with $\text{Var}(h) = \sigma^2$, and maximal wavenumber K. Let $\Gamma = \lfloor KL/\pi \rfloor$. Then by inspection of (6.4), the largest critical $\tilde{M}_{11}$ value is $2\Gamma\pi\sigma^2/L$, which occurs only for $\beta = 0$, and $\alpha = \pm\Gamma$. The corresponding surface is

$$h(x, y) = \frac{\sigma}{\sqrt{2}}\,e^{i\phi}e^{i\Gamma\pi x/L} + \frac{\sigma}{\sqrt{2}}\,e^{-i\phi}e^{-i\Gamma\pi x/L} = \sigma\sqrt{2}\,\cos\left(\frac{\Gamma\pi x}{L} + \phi\right). \tag{6.7}$$

Hence, the surface with the least forward mobility has sinusoidal grooves oriented perpendicular to the direction of the shear stress. The wavelength of the grooves should
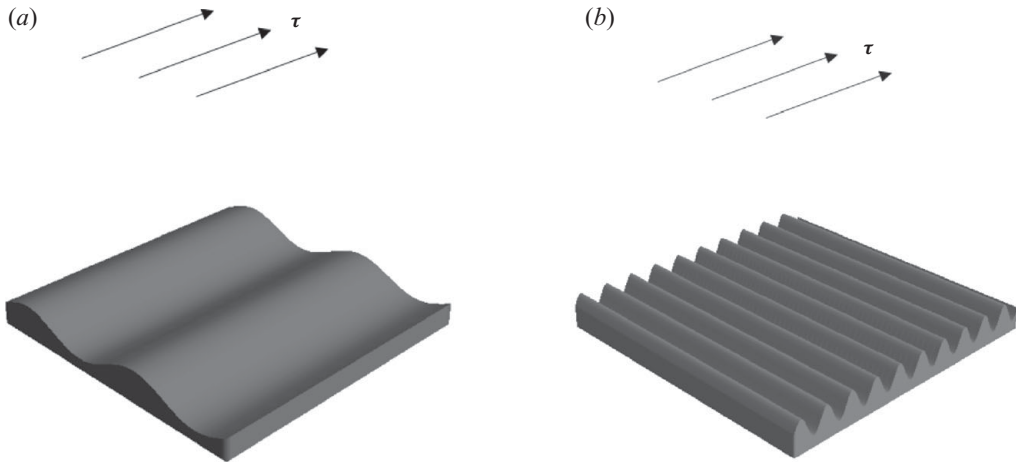
FIGURE 4. (*a*) The periodic surface of fixed variance that restricts flow the least (i.e. maximal forward mobility) has long-wavelength sinusoidal grooves oriented along the direction of the stress. (*b*) The surface of fixed variance that restricts flow the most (i.e. minimal forward mobility) has sinusoidal grooves of the shortest possible wavelength oriented across the direction of the stress.

be the shortest possible, given the fixed surface periodicity and fixed bandwidth. In light of the result from the previous subsection, a very natural symmetry arises in the solutions to maximum/minimum mobility (see figure 4). The overall directionality of the grooves in each case is not surprising – the transverse and parallel distributions are ubiquitous in the optimization of physical properties for a variety of materials (Torquato 2002) – though the groove shape is perhaps less obvious.

7. Random height fluctuations

Next, we move on to the mobility of a randomly textured surface, a problem which has been studied previously in various contexts. Poiseuille flow over surfaces with Gaussian distributed height/wettability was analysed in Kunert & Harting (2008) using a lattice Boltzmann simulation method to quantify the decrease in the effective channel width as the width of the distribution increases. Other work on random texturing has focused on particular surface features, such as Sarkar & Prosperetti (1996), which studies the effect of a random array of compact bumps, and Sbragaglia & Prosperetti (2007), which considers surfaces with a random distribution of perfect-slip patches. Here, we consider no-slip surfaces satisfying the following constraints, but having no other distinguishing features.

(*a*) The surface is $2L$-periodic in x and y.
(*b*) The surface has $\text{Var}(h) = \sigma^2$.
(*c*) The bandwidth of h is finite, with maximal wavenumber K.

Let A be the set of integer pairs (m, n) with the property that $\sqrt{k_m^2 + k_n^2} < K$, $m \geqslant 0$ when $n > 0$, and $m > 0$ whenever $n \leqslant 0$ (see figure 5). Under these definitions, any surface obeying our constraints must be of the form

$$h(x, y) = \hat{h}(0, 0) + \sum_{(m,n)\in A} (\hat{h}(m, n)e^{i(k_m x + k_n y)} + \hat{h}(m, n)^* e^{-i(k_m x + k_n y)}) \tag{7.1}$$
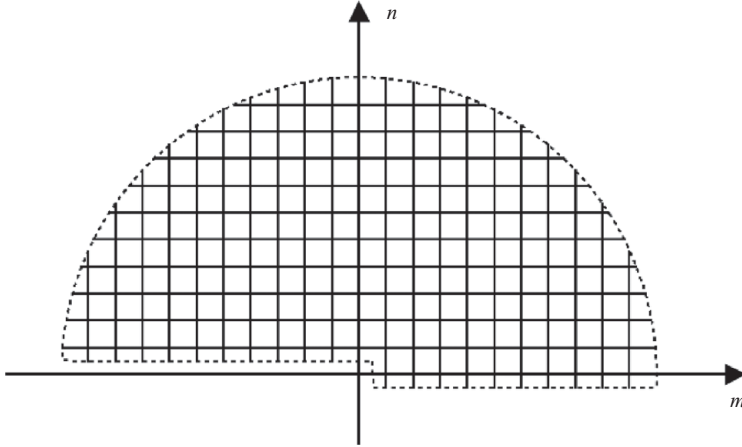
FIGURE 5. The integer grid points within an upward semicircle, excluding the non-positive m-axis, compose the set A. Up to an additive constant, any periodic surface of finite bandwidth can be uniquely described by determining $\hat{h}(m, n)$ on A.

and satisfy

$$\sum_{(m,n)\in A} 2|\hat{h}(m, n)|^2 = \sigma^2. \tag{7.2}$$

Observing the slip matrix formula (3.3), the mobilities depend only on the magnitude of the Fourier coefficients. This suggests a simple, broad probability distribution for sampling the surfaces as shall be described next. First, index the members of A by $\boldsymbol{p}_1, \ldots, \boldsymbol{p}_{|A|}$ and define $\gamma_j \equiv 2|\hat{h}(\boldsymbol{p}_j)|^2$. The region of space in the variables $\{\gamma_1, \ldots, \gamma_{|A|}\}$ that fulfils the constraint on the variance is

$$0 \leqslant \gamma_1 \leqslant \sigma^2, \tag{7.3a}$$

$$0 \leqslant \gamma_2 \leqslant \sigma^2 - \gamma_1, \tag{7.3b}$$

$$0 \leqslant \gamma_3 \leqslant \sigma^2 - \gamma_1 - \gamma_2, \tag{7.3c}$$

$$\vdots$$

$$0 \leqslant \gamma_{|A|-1} \leqslant \sigma^2 - \sum_{j=1}^{|A|-2} \gamma_j, \tag{7.3d}$$

$$\gamma_{|A|} = \sigma^2 - \sum_{j=1}^{|A|-1} \gamma_j. \tag{7.3e}$$

Let us denote by Ω the higher dimensional tetrahedron described by the above constraints on $\gamma_1, \ldots, \gamma_{|A|-1}$. That is, a surface h obeying our constraints is equivalently one point in the region Ω. One probability distribution we can write is

$$\left\{ \begin{array}{l} \text{Prob. of } \mathrm{h} \in \Omega \text{ with } \gamma \text{ values between} \\ \gamma_j \text{ and } \gamma_j + \mathrm{d}\gamma_j \text{ for each } 1 < \mathrm{j} < |\mathrm{A}| - 1 \end{array} \right\} = \prod_{j=1}^{|A|-1} d\gamma_j \bigg/ \left(\int_{\Omega} \prod_{j=1}^{|A|-1} \mathrm{d}\gamma_j \right). \tag{7.4}$$

Under this distribution, the probability of choosing some surface within a subset of Ω occurs with probability proportional to the volume of that subset. Using an

overbar to denote the weighted average by this distribution, a direct integration using limits defined by (7.3) gives

$$\overline{\sum_{j=1}^{|A|} f(\boldsymbol{p}_j)\gamma_j} = \frac{\int_\Omega \left(\sum_{j=1}^{|A|} f(\boldsymbol{p}_j)\gamma_j \right) \mathrm{d}\gamma_1 \, \mathrm{d}\gamma_2 \, \cdots \, \mathrm{d}\gamma_{|A|-1}}{\int_\Omega \mathrm{d}\gamma_1 \, \mathrm{d}\gamma_2 \, \cdots \, \mathrm{d}\gamma_{|A|-1}} = \frac{\sigma^2}{|A|} \sum_{j=1}^{|A|} f(\boldsymbol{p}_j) \tag{7.5}$$

for any function f. Applying this to (3.4), one finds

$$\overline{\tilde{\boldsymbol{M}}} = \frac{\sigma^2}{|A|} \begin{pmatrix} \displaystyle\sum_{(m,n)\in A} \frac{2k_m^2 + k_n^2}{\sqrt{k_m^2 + k_n^2}} & \displaystyle\sum_{(m,n)\in A} \frac{k_m k_n}{\sqrt{k_m^2 + k_n^2}} \\[2ex] \displaystyle\sum_{(m,n)\in A} \frac{k_m k_n}{\sqrt{k_m^2 + k_n^2}} & \displaystyle\sum_{(m,n)\in A} \frac{k_m^2 + 2k_n^2}{\sqrt{k_m^2 + k_n^2}} \end{pmatrix}. \tag{7.6}$$

Each sum in the matrix above can be approximated by the semicircular integral

$$\sum_{(m,n)\in A} f(m,n) \cong \int_{r=0}^{KL/\pi} \int_{\theta=0}^{\pi} f(r\cos\theta, r\sin\theta)\, r \, \mathrm{d}r \, \mathrm{d}\theta$$

due to symmetry along the m-axis and the fact the $f(0,0)=0$ for each summand. Then we may write

$$\overline{\tilde{\boldsymbol{M}}} \cong \frac{\sigma^2}{|A|} \begin{pmatrix} \dfrac{K^3 L^2}{2\pi} & 0 \\[2ex] 0 & \dfrac{K^3 L^2}{2\pi} \end{pmatrix} = \sigma^2 \frac{K^3 L^2}{2\pi|A|} \boldsymbol{1}, \tag{7.7}$$

where $\boldsymbol{1}$ is the 2×2 identity tensor. Lastly, the number of elements in A can be computed with a semicircular area approximation (excluding the missing point at the origin):

$$|A| \cong \tfrac{1}{2}\pi (KL/\pi)^2 - 1,$$

giving the final result

$$\overline{\tilde{\boldsymbol{M}}} \cong \sigma^2 \frac{K^3 L^2}{K^2 L^2 - 2\pi} \boldsymbol{1} \cong \sigma^2 K \boldsymbol{1}. \tag{7.8}$$

where the last approximation holds for KL large enough.

As expected, a random surface of fixed variance and bandwidth has isotropic slip properties. Moreover, the forward mobility of a random surface is approximately $-\epsilon^2 \sigma^2 K$ which fits nicely into the ordering we find for the most and least optimal surfaces of fixed variance as discussed in §6:

$$\text{forward mobility:} \qquad \underbrace{-\epsilon^2 \sigma^2 \frac{\pi}{L}}_{\text{most}} < \underbrace{-\epsilon^2 \sigma^2 K}_{\text{random}} < \underbrace{-2\epsilon^2 \sigma^2 \frac{\Gamma\pi}{L}}_{\text{least}}.$$

Or perhaps the ordering is easier to see in terms of the relative sizes of these three quantities, which is closely approximated by

$$\text{most : random : least} \cong -(1 : \Gamma : 2\Gamma).$$

We reiterate that the result for mean mobility over a random surface depends entirely on the choice of the probability distribution. We have selected a particular one, which

is simple enough to perform the necessary calculations, and which appears relatively unbiased towards any particular subset of surfaces.

8. Surfaces with fluctuating scalar Navier slip

Up to this point, the focus has been on surface patterns due solely to height fluctuations. Now, let us expand the analysis to surfaces that have fluctuating scalar slip properties, such as composite surfaces where each material has different hydrophobicity.

Such surfaces can be described with a scalar Navier slip boundary condition, which relates the fluid slip along the surface to the fluid shear rate at the surface

$$\boldsymbol{u}^s = b(x, y) \frac{\partial \boldsymbol{u}}{\partial n}. \tag{8.1}$$

In this section, we analyse the macroscopic flow properties of surfaces with slip coefficient $\epsilon b(x, y)$ measuring small variations from no-slip, as well as possible height fluctuations $\epsilon h(x, y)$, both of the same periodicity. Applying the Navier slip condition along the surface $\epsilon h(x, y)$ gives

$$\boldsymbol{u}(x, y, \epsilon h(x, y)) = \epsilon b(x, y) \frac{(-\epsilon h_x, -\epsilon h_y, 1)}{|(-\epsilon h_x, -\epsilon h_y, 1)|} \cdot \nabla \boldsymbol{u} \Big|_{z=\epsilon h(x,y)}. \tag{8.2}$$

Adopting the perturbation series representations of $\boldsymbol{u}$ and p from § 3.1, one expands in ϵ to yield the following term-by-term conditions for the flow at $z = 0$:

$$\boldsymbol{u}_0(x, y, 0) = \boldsymbol{0}, \tag{8.3}$$

$$\boldsymbol{u}_1(x, y, 0) = (b(x, y) - h(x, y)) \frac{\partial \boldsymbol{u}_0}{\partial z} \Big|_{z=0}, \tag{8.4}$$

$$\boldsymbol{u}_2(x, y, 0) = -h(x, y) \frac{\partial \boldsymbol{u}_1}{\partial z} \Big|_{z=0} - \frac{h(x, y)^2}{2} \frac{\partial^2 \boldsymbol{u}_0}{\partial z^2} \Big|_{z=0} \tag{8.5}$$

$$+ b(x, y) \left(h(x, y) \frac{\partial^2 \boldsymbol{u}_0}{\partial z^2} + \left(-h_x \frac{\partial \boldsymbol{u}_0}{\partial x} \Big|_{z=0}, -h_y \frac{\partial \boldsymbol{u}_0}{\partial y} \Big|_{z=0}, 1 \right) \cdot \nabla \boldsymbol{u}_1 \Big|_{z=0} \right). \tag{8.6}$$

The $z = \infty$ conditions are the same as those in § 3.1. The term $\boldsymbol{u}_0$ is solved, as before, by

$$\boldsymbol{u}_0(x, y, z) = \boldsymbol{\tau} z. \tag{8.7}$$

Substituting this result into the above boundary conditions for the other orders, one finds

$$\boldsymbol{u}_1(x, y, 0) = (b(x, y) - h(x, y)) \boldsymbol{\tau}, \tag{8.8}$$

$$\boldsymbol{u}_2(x, y, 0) = (b(x, y) - h(x, y)) \frac{\partial \boldsymbol{u}_1}{\partial z} \Big|_{z=0}. \tag{8.9}$$

Comparing to §§ 3.3 and 3.4, it is now evident that these boundary conditions are the same as the previous, except with the switch $h(x, y) \to h(x, y) - b(x, y)$. Hence, the solution up to second order can be inferred directly by modifying the results of the previous sections.

Applying the switch and writing, as before, in terms of the variable $\tilde{z} = z - \epsilon \langle h(x, y) \rangle$, one obtains the slip relation

$$\boldsymbol{u}^s = \epsilon \langle b(x, y) \rangle \boldsymbol{\tau} - \epsilon^2 \tilde{\boldsymbol{M}}(h - b) \cdot \boldsymbol{\tau} + O(\epsilon^3). \tag{8.10}$$

Up to second order, the effective slip of a surface with small scalar slip and height fluctuations is the same as that of a no-slip surface except with $h \rightarrow h - b$ in the argument of $\tilde{\boldsymbol{M}}$, plus an isotropic first-order term due to the average of b. This form is reminiscent of the result for sinusoidal surfaces with constant Navier slip detailed in Panzer *et al.* (1992).

8.1. *A simple optimization for surfaces with height and Navier slip fluctuations*

Consider a surface with height and slip fluctuations of the same periodicity. The forward mobility, as computed from (8.10), is

$$\frac{\boldsymbol{u}^s \cdot \boldsymbol{\tau}}{|\boldsymbol{\tau}|^2} \approx \epsilon \langle b(x, y) \rangle - \epsilon^2 \frac{\boldsymbol{\tau} \cdot \tilde{\boldsymbol{M}}(h - b) \cdot \boldsymbol{\tau}}{|\boldsymbol{\tau}|^2}. \tag{8.11}$$

Holding the average of $b(x, y)$ fixed, the mobility can be maximized by observing the second-order term above. As per the definition of $\tilde{\boldsymbol{M}}$ (3.4), the mobility matrix is positive definite if $b(x, y) - h(x, y) \neq$ const., and $\boldsymbol{0}$ otherwise. Consequently, the mobility is maximized when $b(x, y) - h(x, y) =$ const. For any given $h(x, y)$, the optimal choice of $b(x, y)$ is

$$b(x, y) - \langle b(x, y) \rangle = h(x, y) - \langle h(x, y) \rangle, \tag{8.12}$$

which gives a mobility of $\epsilon \langle b(x, y) \rangle$. Physically speaking, this means the forward slip is maximized when the peaks of the surface h are more hydrophobic, and the valleys of the surface are more hydrophilic.

9. Conclusion

This work has derived a second-order accurate formula (see (3.3) and (3.4)) describing an effective local boundary condition for shear flows over small-fluctuation periodic surfaces. The formula represents a tensorial mobility law, and is easily extended to include surfaces of both non-uniform hydrophobicity and height changes (defined in (8.10)). We have gone to great lengths to quantify the error of the approximation, so as to provide guidelines for its appropriate usage. Within these guidelines, the formula was optimized in a Lagrange multiplier framework to derive the no-slip surfaces of fixed variance that maximize/minimize the forward mobility. These extremal cases were favourably compared with the mobility of a random, fixed-variance surface as computed by summing over some unbiased distribution. We have also performed a simple optimization that instructs the optimal coupling between height and scalar slip fluctuations when both surface effects can take place.

In the future, we hope to augment our analysis to include the possibility of a surface charge profile. This addition would be useful in electro-kinetic applications to help understand and predict electro-osmotic fluid transport. We also continue from a mathematical perspective to work on enhanced solution methods that may improve the breadth of applicability of the mobility formula.

Appendix A. General solution to the Stokes equations

In this appendix, a general solution to the Stokes equations is given for use in solving the first- and second-order terms in the perturbation expansion displayed in §3.1. It is expressed as a Fourier series in the horizontal dimensions with three

undetermined coefficient sets:

$$u(x, y, z) = \alpha + \sum_{(m,n) \neq \mathbf{0}} e^{i(k_m x + k_n y)} \frac{e^{-z\sqrt{k_m^2 + k_n^2}}}{3\sqrt{k_m^2 + k_n^2}} \left[-ik_m \left(1 + 2z\sqrt{k_m^2 + k_n^2}\right) A(m, n) \right.$$

$$+ \frac{3k_n^2 \sqrt{k_m^2 + k_n^2} - 2k_m^4 z + 2k_m^2 \left(\sqrt{k_m^2 + k_n^2} - k_n^2 z\right)}{k_m^2 + k_n^2} B(m, n)$$

$$\left. - \frac{k_m k_n \left(\sqrt{k_m^2 + k_n^2} - 2z(k_m^2 + k_n^2)\right)}{k_m^2 + k_n^2} C(m, n) \right],$$

$$v(x, y, z) = \beta + \sum_{(m,n) \neq \mathbf{0}} e^{i(k_m x + k_n y)} \frac{e^{-z\sqrt{k_m^2 + k_n^2}}}{3\sqrt{k_m^2 + k_n^2}} \left[-ik_n \left(1 + 2z\sqrt{k_m^2 + k_n^2}\right) A(m, n) \right.$$

$$- \frac{k_m k_n \left(\sqrt{k_m^2 + k_n^2} - 2z(k_m^2 + k_n^2)\right)}{k_m^2 + k_n^2} B(m, n)$$

$$\left. + \frac{3k_m^2 \sqrt{k_m^2 + k_n^2} - 2k_n^4 z + 2k_n^2 \left(\sqrt{k_m^2 + k_n^2} - k_m^2 z\right)}{k_m^2 + k_n^2} C(m, n) \right],$$

$$w(x, y, z) = \gamma + \sum_{(m,n) \neq \mathbf{0}} e^{i(k_m x + k_n y)} \frac{e^{-z\sqrt{k_m^2 + k_n^2}}}{3} \left[\left(3 + 2z\sqrt{k_m^2 + k_n^2}\right) A(m, n) \right.$$

$$\left. - 2ik_m z B(x, y) - 2ik_n z C(m, n) \right],$$

$$p(x, y, z) = \delta + \sum_{(m,n) \neq \mathbf{0}} e^{i(k_m x + k_n y)} \frac{e^{-z\sqrt{k_m^2 + k_n^2}}}{3} \left[4\sqrt{k_m^2 + k_n^2} A(m, n) \right.$$

$$\left. - 4ik_m B(m, n) - 4ik_n C(m, n) \right].$$

This system can be inverted to uniquely determine the constants α, β, γ and the coefficient sets $A(m, n)$, $B(m, n)$, $C(m, n)$ in terms of the chosen lower boundary condition on the velocity, $\mathbf{u}(x, y, 0)$. This general solution always satisfies the following boundary conditions for the first- and second-order perturbation terms:

$$\mathbf{u}(x, y, z) = \mathbf{u}(x + L_x, y + L_y, z), \quad p(x, y, z) = p(x + L_x, y + L_y, z), \quad \left. \frac{\partial \mathbf{u}}{\partial z} \right|_{z=\infty} = \mathbf{0}.$$

Appendix B. Determining error bounds

This appendix derives the error bound displayed as (4.4) in §4.2. To begin, define the following norm on scalar, vector or tensor fields $\mathbf{f}(x, y)$ over a two-dimensional periodic domain:

$$\| \mathbf{f}(x, y) \|_{x,y} = \sqrt{ \frac{1}{4 L_x L_y} \int_{-L_x}^{L_x} \int_{-L_y}^{L_y} |\mathbf{f}(x, y)|^2 \, \mathrm{d}x \, \mathrm{d}y }. \tag{B 1}$$

We reserve $|\cdot|$ for the absolute value (if applied to a scalar) or Euclidean norm (if applied to a vector or matrix). The above is directly proportional to the compact support L_2 norm on functions. The choice of this norm greatly simplifies the analysis since it connects directly to an inner product, and consequently an array of useful theorems.

The exact flow solution in our problem satisfies the no-slip condition along the surface, i.e. $\boldsymbol{u}(x, y, \epsilon h(x, y)) = \boldsymbol{0}$. To measure how much our second-order flow approximation differs from the true solution along the surface, we use the norm to measure the surface error:

$$\text{surface error} = \|\boldsymbol{u}_0(x, y, \epsilon h(x, y)) + \epsilon \boldsymbol{u}_1(x, y, \epsilon h(x, y)) + \epsilon^2 \boldsymbol{u}_2(x, y, \epsilon h(x, y))\|_{x,y}.$$
(B 2)

From Taylor's Remainder Theorem, we know

$$\boldsymbol{u}_1(x, y, \epsilon h) = \boldsymbol{u}_1(x, y, 0) + \epsilon h \left.\frac{\partial \boldsymbol{u}_1}{\partial z}\right|_{z=0} + \int_0^{\epsilon h(x,y)} (\epsilon h(x, y) - z)\frac{\partial^2 \boldsymbol{u}_1}{\partial z^2}\,\mathrm{d}z,$$

$$\boldsymbol{u}_2(x, y, \epsilon h) = \boldsymbol{u}_2(x, y, 0) + \int_0^{\epsilon h(x,y)} \frac{\partial \boldsymbol{u}_2}{\partial z}\,\mathrm{d}z.$$

Inserting these forms into the above, and using the order-by-order boundary conditions to cancel terms, one obtains

$$\text{surface error} = \left\|\epsilon \left(\int_0^{\epsilon h(x,y)} (\epsilon h(x, y) - z)\frac{\partial^2 \boldsymbol{u}_1}{\partial z^2}\,\mathrm{d}z\right) + \epsilon^2 \left(\int_0^{\epsilon h(x,y)} \frac{\partial \boldsymbol{u}_2}{\partial z}\,\mathrm{d}z\right)\right\|_{x,y}$$

$$\leqslant \epsilon \underbrace{\left\|\int_0^{\epsilon h(x,y)} (\epsilon h(x, y) - z)\frac{\partial^2 \boldsymbol{u}_1}{\partial z^2}\,\mathrm{d}z\right\|_{x,y}}_{\equiv R^{(1)}} + \epsilon^2 \underbrace{\left\|\int_0^{\epsilon h(x,y)} \frac{\partial \boldsymbol{u}_2}{\partial z}\,\mathrm{d}z\right\|_{x,y}}_{\equiv R^{(2)}} \quad \text{(B 3)}$$

by the triangle inequality.

To place an upper bound on the error, we must calculate tight bounds on each of these two integrals given any surface $h(x, y)$. This is a highly non-trivial task. As is derived in Appendix C, with judicious use of Parseval's theorem and the Cauchy–Schwarz inequality, we can show that

$$R^{(1)} \equiv \left\|\int_0^{\epsilon h(x,y)} (\epsilon h(x, y) - z)\frac{\partial^2 \boldsymbol{u}_1}{\partial z^2}\,\mathrm{d}z\right\|_{x,y} \leqslant \epsilon^2 h_M^2 K_1 |\boldsymbol{\tau}| \,\|\nabla\nabla h(x, y)\|_{x,y}, \quad \text{(B 4)}$$

$$R^{(2)} \equiv \left\|\int_0^{\epsilon h(x,y)} \frac{\partial \boldsymbol{u}_2}{\partial z}\,\mathrm{d}z\right\|_{x,y} \leqslant \epsilon h_M K_2 |\boldsymbol{\tau}| \big(|\nabla h|_M \|\nabla h(x, y)\|_{x,y} + h_M \|\nabla\nabla h(x, y)\|_{x,y}\big), \quad \text{(B 5)}$$

where K_1 and K_2 are order-1, known, dimensionless constants independent of the choice of ϵ, $\boldsymbol{\tau}$, or $h(x, y)$, and for any function $f(x, y)$ we adopt the notation

$$f_M \equiv \max_{x,y} f(x, y). \quad \text{(B 6)}$$

The bounds on $R^{(1)}$ and $R^{(2)}$ applied to (B 3) give

$$\text{surface error} \leqslant \kappa \epsilon^3 h_M |\boldsymbol{\tau}| (h_M \|\nabla\nabla h(x, y)\|_{x,y} + |\nabla h|_M \|\nabla h(x, y)\|_{x,y})$$

$$\leqslant \kappa \epsilon^3 h_M |\boldsymbol{\tau}| \big(h_M |\nabla\nabla h|_M + |\nabla h|_M^2\big) \equiv \text{surface error bound}, \quad \text{(B 7)}$$

where we define $\kappa \equiv K_1 + K_2$, which is another known order-1 constant.

Next, we make the connection between the surface error and the error in the predicted slip. The exact flow solution must have the velocity go to zero along the surface. The second-order approximation that we have found has some fallacious extra velocity along the surface that arises due to truncation error, and the surface error

is a space-average measurement of this erroneous surface speed. If we let $\boldsymbol{u}(x, y, z)$ represent the true solution, $\boldsymbol{u}^{app}(x, y, z) = \boldsymbol{u}_0(x, y, z) + \epsilon \boldsymbol{u}_1(x, y, z) + \epsilon^2 \boldsymbol{u}_2(x, y, z)$ be our second-order approximation, and $\Delta(x, y, z) \equiv \boldsymbol{u}(x, y, z) - \boldsymbol{u}^{app}(x, y, z)$, it follows that

$$\| \Delta(x, y, \epsilon h(x, y)) \|_{x, y} \leqslant \text{surface error bound}. \tag{B 8}$$

Since both $\boldsymbol{u}(x, y, z)$ and $\boldsymbol{u}^{app}(x, y, z)$ obey the Stokes equations exactly, the difference $\Delta(x, y, z)$ must also obey the Stokes equations. Moreover, since both $\boldsymbol{u}$ and $\boldsymbol{u}^{app}$ satisfy the same traction boundary condition as $z \to \infty$, then the difference flow $\Delta(x, y, z)$ must asymptote to a constant uniform flow (zero shear traction) for large z. The speed in the uniform flow region is precisely the error in the approximation for the effective slip. Our goal is hence reduced to determining the maximum possible flow speed that can occur at large z in a Stokes flow $\Delta(x, y, z)$ that obeys (B 8) and zero shear tractions at $z = \infty$.

While the total surface error is described by (B 7), the distribution of this extra velocity over the surface is undetermined, providing the only degree of freedom in this maximization. We state without proof that the maximal large-z uniform flow arises for

$$\Delta(x, y, z) = (\text{surface error bound})\, \boldsymbol{e}, \tag{B 9}$$

where $\boldsymbol{e}$ is any horizontal unit vector. In other words, Δ has a large-z uniform flow of maximal speed when the extra surface velocity represented by the surface error is equally distributed and uniformly directed along the surface, so that $\Delta(x, y, z)$ is globally uniform. This choice of Δ saturates (B 8).

Recalling the definition in (B 7), the above selection of $\Delta(x, y, z)$ implies the error in the second-order slip approximation is subject to

$$|\boldsymbol{u}^s - (-\epsilon^2 \tilde{\boldsymbol{M}}(h) \cdot \boldsymbol{\tau})| \leqslant \epsilon^3 \kappa h_M |\boldsymbol{\tau}| \left(h_M |\nabla \nabla h|_M + |\nabla h|_M^2 \right),$$

which is our desired result.

Appendix C. Bounding the integrals $R^{(1)}$ and $R^{(2)}$

The purpose of this appendix is to rigorously prove the bounds on the error quantities $R^{(1)}$ and $R^{(2)}$ shown as (B 4) and (B 5) in Appendix B.

C.1. *The error* $R^{(1)}$

We begin with the bound on $R^{(1)}$. First, we observe by the Cauchy–Schwarz inequality that

$$\left| \int_0^{\epsilon h(x, y)} (\epsilon h(x, y) - z) \frac{\partial^2 \boldsymbol{u}_1}{\partial z^2} \, \mathrm{d}z \right| \leqslant \sqrt{\int_0^{\epsilon h(x, y)} \left| (\epsilon h(x, y) - z) \frac{\partial^2 \boldsymbol{u}_1}{\partial z^2} \right|^2 \mathrm{d}z} \sqrt{\int_0^{\epsilon h(x, y)} 1^2 \, \mathrm{d}z}$$

$$\leqslant \sqrt{\epsilon h(x, y)} \sqrt{\int_0^{\epsilon h(x, y)} (\epsilon h(x, y) - z)^2 \left| \frac{\partial^2 \boldsymbol{u}_1}{\partial z^2} \right|^2 \mathrm{d}z}$$

$$\leqslant \sqrt{\epsilon h_M} \sqrt{\int_0^{\epsilon h_M} (\epsilon h_M - z)^2 \left| \frac{\partial^2 \boldsymbol{u}_1}{\partial z^2} \right|^2 \mathrm{d}z}.$$

We insert this result into the definition of $R^{(1)}$, and expand the function norm:

$$
R^{(1)} \leqslant \left\| \sqrt{\epsilon h_M} \sqrt{\int_0^{\epsilon h_M} (\epsilon h_M - z)^2 \left| \frac{\partial^2 \boldsymbol{u}_1}{\partial z^2} \right|^2 \mathrm{d}z} \right\|_{x,y}
$$

$$
= \sqrt{\frac{1}{4L_x L_y} \int_{-L_x}^{L_x} \int_{-L_y}^{L_y} \epsilon h_M \left(\int_0^{\epsilon h_M} (\epsilon h_M - z)^2 \left| \frac{\partial^2 \boldsymbol{u}_1}{\partial z^2} \right|^2 \mathrm{d}z \right) \mathrm{d}x \, \mathrm{d}y}
$$

$$
= \sqrt{\epsilon h_M \int_0^{\epsilon h_M} (\epsilon h_M - z)^2 \left\| \frac{\partial^2 \boldsymbol{u}_1}{\partial z^2} \right\|_{x,y}^2 \mathrm{d}z}. \tag{C 1}
$$

The final line follows from rearranging the order of integration. In order to apply the next step, we must first compute $|\partial^2 \boldsymbol{u}_1 / \partial z^2|^2$, which is straightforward because $\boldsymbol{u}_1(x, y, z)$ is completely known. The result is lengthy, but can be written somewhat compactly as

$$
\left| \frac{\partial^2 \boldsymbol{u}_1}{\partial z^2} \right|^2 = \left(\frac{\partial^2 u_1}{\partial z^2} \right)^2 + \left(\frac{\partial^2 v_1}{\partial z^2} \right)^2 + \left(\frac{\partial^2 w_1}{\partial z^2} \right)^2
$$

$$
= \sum_{j=\{1,2,3\}} \left(\sum_{(m,n)\neq \boldsymbol{0}} \boldsymbol{\tau} \cdot (\boldsymbol{q}_{m,n} \cdot \boldsymbol{A}_{(j)} \cdot \boldsymbol{p}_{m,n}, \quad \boldsymbol{q}_{m,n} \cdot \boldsymbol{B}_{(j)} \cdot \boldsymbol{p}_{m,n}) \right.
$$

$$
\left. \times \mathrm{e}^{-z\sqrt{k_m^2 + k_n^2}} \hat{h}(m, n) \mathrm{e}^{\mathrm{i}(k_m x + k_n y)} \right)^2,
$$

where for each choice of m and n, $\boldsymbol{q}_{m,n}$ and $\boldsymbol{p}_{m,n}$ are the vectors defined by

$$
\left.
\begin{aligned}
\boldsymbol{q}_{m,n} &= \left(1, z\sqrt{k_m^2 + k_n^2}, zk_m, zk_n \right), \\
\boldsymbol{p}_{m,n} &= \left(k_m^2, k_n^2, \sqrt{2}k_m k_n, k_m\sqrt{k_m^2 + k_n^2}, k_n\sqrt{k_m^2 + k_n^2} \right),
\end{aligned}
\right\} \tag{C 2}
$$

and for each j, $\boldsymbol{A}_{(j)}$ and $\boldsymbol{B}_{(j)}$ are constant, dimensionless, 4×5 matrices of order 1 in size.

Now for the crucial step: apply Parseval's theorem to convert the function norm to a discrete sum,

$$
\left\| \frac{\partial^2 \boldsymbol{u}_1}{\partial z^2} \right\|_{x,y}^2 = \frac{1}{4L_x L_y} \int_{-L_x}^{L_x} \int_{-L_y}^{L_y} \left| \frac{\partial^2 \boldsymbol{u}_1}{\partial z^2} \right|^2 \mathrm{d}x \, \mathrm{d}y
$$

$$
= \sum_{j=\{1,2,3\}} \left[\frac{1}{4L_x L_y} \int_{-L_x}^{L_x} \int_{-L_y}^{L_y} \left(\sum_{(m,n)\neq \boldsymbol{0}} \boldsymbol{\tau} \cdot (\boldsymbol{q}_{m,n} \cdot \boldsymbol{A}_{(j)} \cdot \boldsymbol{p}_{m,n}, \quad \boldsymbol{q}_{m,n} \cdot \boldsymbol{B}_{(j)} \cdot \boldsymbol{p}_{m,n}) \right. \right.
$$

$$
\left. \left. \times \mathrm{e}^{-z\sqrt{k_m^2 + k_n^2}} \hat{h}(m, n) \mathrm{e}^{\mathrm{i}(k_m x + k_n y)} \right)^2 \right] \mathrm{d}x \, \mathrm{d}y
$$

$$
= \sum_{j=\{1,2,3\}} \sum_{(m,n)\neq \boldsymbol{0}} \left| \boldsymbol{\tau} \cdot (\boldsymbol{q}_{m,n} \cdot \boldsymbol{A}_{(j)} \cdot \boldsymbol{p}_{m,n}, \quad \boldsymbol{q}_{m,n} \cdot \boldsymbol{B}_{(j)} \cdot \boldsymbol{p}_{m,n}) \mathrm{e}^{-z\sqrt{k_m^2 + k_n^2}} \hat{h}(m, n) \right|^2
$$

$$
\leqslant \sum_{j=\{1,2,3\}} \sum_{(m,n)\neq \boldsymbol{0}} |\boldsymbol{\tau}|^2 |\boldsymbol{q}_{m,n}|^2 (|\boldsymbol{A}_{(j)}|^2 + |\boldsymbol{B}_{(j)}|^2) |\boldsymbol{p}_{m,n}|^2 \, \mathrm{e}^{-2z\sqrt{k_m^2 + k_n^2}} |\hat{h}(m, n)|^2.
$$

The last line follows from the Cauchy–Schwarz inequality. To express the result more simply, define

$$\alpha = \sum_{j=\{1,2,3\}} |A_{(j)}|^2 + |B_{(j)}|^2.$$

Then, expanding the norms on the vectors p and q, we have

$$\left\| \frac{\partial^2 u_1}{\partial z^2} \right\|_{x,y}^2 \leqslant \alpha |\tau|^2 \sum_{(m,n)\neq 0} \left(1 + z^2 \left(2k_m^2 + 2k_n^2\right)\right) \left(2k_m^4 + 2k_n^4 + 4k_m^2 k_n^2\right) e^{-2z\sqrt{k_m^2 + k_n^2}} |\hat{h}(m,n)|^2.$$
(C 3)

With a bound on the integrand in (C 1) now established, we move on to evaluate the integral

$$\int_0^{\epsilon h_M} (\epsilon h_M - z)^2 \left\| \frac{\partial^2 u_1}{\partial z^2} \right\|_{x,y}^2 \, dz \leqslant \int_0^{\epsilon h_M} \left[(\epsilon h_M - z)^2 \alpha |\tau|^2 \sum_{(m,n)\neq 0} \left(1 + z^2 \left(2k_m^2 + 2k_n^2\right)\right) \right.$$
$$\left. \times \left(2k_m^4 + 2k_n^4 + 4k_m^2 k_n^2\right) e^{-2z\sqrt{k_m^2 + k_n^2}} |\hat{h}(m,n)|^2 \right] dz$$
$$= 2\alpha |\tau|^2 \sum_{(m,n)\neq 0} \left(k_m^4 + k_n^4 + 2k_m^2 k_n^2\right) |\hat{h}(m,n)|^2$$
$$\times \left[\int_0^{\epsilon h_M} (\epsilon h_M - z)^2 e^{-2z\sqrt{k_m^2 + k_n^2}} \, dz \right.$$
$$\left. + 2\left(k_m^2 + k_n^2\right) \int_0^{\epsilon h_M} (\epsilon h_M - z)^2 z^2 e^{-2z\sqrt{k_m^2 + k_n^2}} \, dz \right]. \quad \text{(C 4)}$$

Now we bound the two z integrals appearing in the last expression. One can show by basic calculus that for any $z \geqslant 0$,

$$e^{-2z\sqrt{k_m^2 + k_n^2}} \leqslant 1 \quad \text{and} \quad z^2 e^{-2z\sqrt{k_m^2 + k_n^2}} \leqslant \frac{4}{e^2 \left(k_m^2 + k_n^2\right)}. \quad \text{(C 5)}$$

Hence,

$$\int_0^{\epsilon h_M} (\epsilon h_M - z)^2 e^{-2z\sqrt{k_m^2 + k_n^2}} \, dz \leqslant \int_0^{\epsilon h_M} (\epsilon h_M - z)^2 \, dz = \frac{\epsilon^3 h_M^3}{3}$$

and

$$\int_0^{\epsilon h_M} (\epsilon h_M - z)^2 z^2 e^{-2z\sqrt{k_m^2 + k_n^2}} \, dz \leqslant \frac{4}{e^2 \left(k_m^2 + k_n^2\right)} \int_0^{\epsilon h_M} (\epsilon h_M - z)^2 \, dz = \frac{4\epsilon^3 h_M^3}{3e^2 \left(k_m^2 + k_n^2\right)}.$$

Substituting these bounds in (C 4), we obtain

$$\int_0^{\epsilon h_M} (\epsilon h_M - z) \left\| \frac{\partial^2 u_1}{\partial z^2} \right\|_{x,y}^2 \, dz \leqslant \epsilon^3 h_M^3 |\tau|^2 K_1^2 \sum_{(m,n)\neq 0} \left(k_m^4 + k_n^4 + 2k_m^2 k_n^2\right) |\hat{h}(m,n)|^2, \quad \text{(C 6)}$$

where $K_1 \equiv \sqrt{2\alpha(1 + 8/e^2)/3}$. Now, observe that

$$
\sum_{(m,n)\neq \mathbf{0}} \left(k_m^4 + k_n^4 + 2k_m^2 k_n^2\right) |\hat{h}(m,n)|^2
$$

$$
= \sum_{(m,n)\neq \mathbf{0}} k_m^4 |\hat{h}(m,n)|^2 + \sum_{(m,n)\neq \mathbf{0}} k_n^4 |\hat{h}(m,n)|^2 + 2 \sum_{(m,n)\neq \mathbf{0}} k_m^2 k_n^2 |\hat{h}(m,n)|^2
$$

$$
= \sum_{(m,n)\neq \mathbf{0}} \left| -k_m^2 \hat{h}(m,n) \right|^2 + \sum_{(m,n)\neq \mathbf{0}} \left| -k_n^2 \hat{h}(m,n) \right|^2 + 2 \sum_{(m,n)\neq \mathbf{0}} |-k_m k_n \hat{h}(m,n)|^2
$$

$$
= \left\| \sum_{(m,n)\neq \mathbf{0}} -k_m^2 \hat{h}(m,n) e^{i(k_m x + k_n y)} \right\|^2_{x,y} + \left\| \sum_{(m,n)\neq \mathbf{0}} -k_n^2 \hat{h}(m,n) e^{i(k_m x + k_n y)} \right\|^2_{x,y}
$$

$$
+ 2 \left\| \sum_{(m,n)\neq \mathbf{0}} -k_m k_n \hat{h}(m,n) e^{i(k_m x + k_n y)} \right\|^2_{x,y}
$$

$$
= \left\| \frac{\partial^2 h(x,y)}{\partial x^2} \right\|^2_{x,y} + \left\| \frac{\partial^2 h(x,y)}{\partial y^2} \right\|^2_{x,y} + 2 \left\| \frac{\partial^2 h(x,y)}{\partial x \partial y} \right\|^2_{x,y}. \tag{C 7}
$$

Parseval's theorem is invoked in the penultimate line to swap each discrete sum for the function norm of a Fourier series. Substituting (C 7) into (C 6), we may rewrite (C 1) as

$$
R^{(1)} \leqslant \epsilon^2 h_M^2 K_1 |\boldsymbol{\tau}| \sqrt{ \left\| \frac{\partial^2 h(x,y)}{\partial x^2} \right\|^2_{x,y} + \left\| \frac{\partial^2 h(x,y)}{\partial y^2} \right\|^2_{x,y} + 2 \left\| \frac{\partial^2 h(x,y)}{\partial x \partial y} \right\|^2_{x,y} }
$$

$$
= \epsilon^2 h_M^2 K_1 |\boldsymbol{\tau}| \, \|\nabla\nabla h(x,y)\|_{x,y} ,
$$

giving us our final result.

C.2. *The error* $R^{(2)}$

To compute the second error term $R^{(2)}$, one must have the full solution for the second-order velocity $\boldsymbol{u}_2(x,y,z)$. Let C_u, C_v and C_w represent the non-constant-term Fourier coefficients for $\boldsymbol{u}_2(x,y,0)$, obtainable via convolution. That is,

$$
u_2(x,y,0) = -h(x,y) \left. \frac{\partial u_1}{\partial z} \right|_{z=0} = -\hat{\boldsymbol{x}} \cdot \tilde{\boldsymbol{M}} \cdot \boldsymbol{\tau} + \sum_{(m,n)\neq \mathbf{0}} C_u(m,n) e^{i(k_m x + k_n y)}, \tag{C 8}
$$

$$
v_2(x,y,0) = -h(x,y) \left. \frac{\partial v_1}{\partial z} \right|_{z=0} = -\hat{\boldsymbol{y}} \cdot \tilde{\boldsymbol{M}} \cdot \boldsymbol{\tau} + \sum_{(m,n)\neq \mathbf{0}} C_v(m,n) e^{i(k_m x + k_n y)}, \tag{C 9}
$$

$$
w_2(x,y,0) = -h(x,y) \left. \frac{\partial w_1}{\partial z} \right|_{z=0} = \sum_{(m,n)\neq \mathbf{0}} C_w(m,n) e^{i(k_m x + k_n y)}. \tag{C 10}
$$

Fitting these boundary conditions under the general solution, one obtains

$$
u_2 = -\hat{\boldsymbol{x}} \cdot \tilde{\boldsymbol{M}} \cdot \boldsymbol{\tau} + \sum_{(m,n)\neq \mathbf{0}} e^{-z\sqrt{k_m^2 + k_n^2}} \left(\frac{-k_m k_n C_v - k_m^2 C_u}{\sqrt{k_m^2 + k_n^2}} z - \mathrm{i} m z C_w + C_u \right) e^{i(k_m x + k_n y)},
$$

$$
\tag{C 11}
$$

$$v_2 = -\hat{\boldsymbol{y}} \cdot \tilde{\boldsymbol{M}} \cdot \boldsymbol{\tau} + \sum_{(m,n) \neq \boldsymbol{0}} e^{-z\sqrt{k_m^2 + k_n^2}} \left(\frac{-k_m k_n C_u - k_n^2 C_v}{\sqrt{k_m^2 + k_n^2}} z - \mathrm{i} n z C_w + C_v \right) e^{\mathrm{i}(k_m x + k_n y)},$$

$$\tag{C 12}$$

$$w_2 = \sum_{(m,n) \neq \boldsymbol{0}} e^{-z\sqrt{k_m^2 + k_n^2}} \left(\left(\sqrt{k_m^2 + k_n^2} C_w - \mathrm{i} m C_u - \mathrm{i} n C_v \right) z + C_w \right) e^{\mathrm{i}(k_m x + k_n y)}. \tag{C 13}$$

The derivation of the bound on $R^{(2)}$ follows a sequence similar to that of the proof in the last subsection for $R^{(1)}$. Steps will be abbreviated accordingly. First, the Cauchy–Schwarz inequality allows us to bound the integral:

$$\left| \int_0^{\epsilon h(x,y)} \frac{\partial \boldsymbol{u}_2}{\partial z} \, dz \right| \leqslant \sqrt{\epsilon h_M} \sqrt{\int_0^{\epsilon h_M} \left| \frac{\partial \boldsymbol{u}_2}{\partial z} \right|^2 \, \mathrm{d}z}.$$

As in the previous section, the next step is to insert this result into the definition of $R^{(2)}$ and expand the function norm, ultimately giving us

$$R^{(2)} \leqslant \sqrt{\epsilon h_M \int_0^{\epsilon h_M} \left\| \frac{\partial^2 \boldsymbol{u}_2}{\partial z} \right\|_{x,y}^2 \, \mathrm{d}z}. \tag{C 14}$$

Taking the z derivative of $\boldsymbol{u}_2$ and squaring, we find a result of the form

$$\left| \frac{\partial \boldsymbol{u}_2}{\partial z} \right|^2 = \sum_{j=\{1,2,3\}} \left(\sum_{(m,n) \neq \boldsymbol{0}} \boldsymbol{c}_{m,n} \cdot (\boldsymbol{q}_{m,n} \cdot \boldsymbol{D}_{(j)} \cdot \boldsymbol{p}_{m,n}, \boldsymbol{q}_{m,n} \cdot \boldsymbol{E}_{(j)} \cdot \boldsymbol{p}_{m,n}, \boldsymbol{q}_{m,n} \cdot \boldsymbol{F}_{(j)} \cdot \boldsymbol{p}_{m,n}) \right.$$
$$\left. \times \frac{e^{-z\sqrt{k_m^2 + k_n^2}}}{\sqrt{k_m^2 + k_n^2}} e^{\mathrm{i}(k_m x + k_n y)} \right)^2,$$

where the vectors $\boldsymbol{p}_{m,n}$ and $\boldsymbol{q}_{m,n}$ are defined in (C 2), $\boldsymbol{c}_{m,n} = (C_u, C_v, C_w)$, and the matrices $\boldsymbol{D}_{(j)}$, $\boldsymbol{E}_{(j)}$ and $\boldsymbol{F}_{(j)}$ are constant 4×5 matrices for each j.

As was done before, we next apply Parseval's theorem to this result, giving

$$\left\| \frac{\partial \boldsymbol{u}_2}{\partial z} \right\|_{x,y}^2 = \sum_{j=\{1,2,3\}} \sum_{(m,n) \neq \boldsymbol{0}} \left| \frac{e^{-z\sqrt{k_m^2 + k_n^2}}}{\sqrt{k_m^2 + k_n^2}} \right|^2$$
$$\times |\boldsymbol{c}_{m,n} \cdot (\boldsymbol{q}_{m,n} \cdot \boldsymbol{D}_{(j)} \cdot \boldsymbol{p}_{m,n}, \; \boldsymbol{q}_{m,n} \cdot \boldsymbol{E}_{(j)} \cdot \boldsymbol{p}_{m,n}, \; \boldsymbol{q}_{m,n} \cdot \boldsymbol{F}_{(j)} \cdot \boldsymbol{p}_{m,n})|^2.$$

We apply the Cauchy–Schwarz inequality to this result, and simplify/expand algebraically:

$$
\left\| \frac{\partial \boldsymbol{u}_2}{\partial z} \right\|_{x,y}^2 \leqslant \sum_{(m,n)\neq 0} \beta \, |\boldsymbol{c}_{m,n}|^2 |\boldsymbol{p}_{m,n}|^2 |\boldsymbol{q}_{m,n}|^2 \frac{e^{-2z\sqrt{k_m^2+k_n^2}}}{k_m^2+k_n^2}
$$

$$
= \sum_{(m,n)\neq 0} \beta \, |\boldsymbol{c}_{m,n}|^2 |\boldsymbol{p}_{m,n}|^2 \frac{2k_m^4 + 2k_n^4 + 4k_m^2 k_n^2}{k_m^2+k_n^2} e^{-2z\sqrt{k_m^2+k_n^2}}
$$

$$
= \sum_{(m,n)\neq 0} 2\beta \, |\boldsymbol{c}_{m,n}|^2 |\boldsymbol{p}_{m,n}|^2 \left(k_m^2+k_n^2\right) e^{-2z\sqrt{k_m^2+k_n^2}}
$$

$$
= \sum_{(m,n)\neq 0} 2\beta \, |\boldsymbol{c}_{m,n}|^2 \left(1 + 2z^2\left(k_m^2+k_n^2\right)\right)\left(k_m^2+k_n^2\right) e^{-2z\sqrt{k_m^2+k_n^2}},
$$

where

$$
\beta = \sum_{j=\{1,2,3\}} |\boldsymbol{D}_{(j)}|^2 + |\boldsymbol{E}_{(j)}|^2 + |\boldsymbol{F}_{(j)}|^2 .
$$

The integral in (C 14) can now be bounded:

$$
\int_0^{\epsilon h_M} \left\| \frac{\partial \boldsymbol{u}_2}{\partial z} \right\|_{x,y}^2 \mathrm{d}z \leqslant \sum_{(m,n)\neq 0} 2\beta |\boldsymbol{c}_{m,n}|^2 \left(k_m^2+k_n^2\right) \left[\int_0^{\epsilon h_M} e^{-2z\sqrt{k_m^2+k_n^2}} \, \mathrm{d}z + 2\left(k_m^2+k_n^2\right) \right.
$$

$$
\left. \times \int_0^{\epsilon h_M} z^2 e^{-2z\sqrt{k_m^2+k_n^2}} \, \mathrm{d}z \right]
$$

$$
\leqslant \epsilon h_M K_2^2 \sum_{(m,n)\neq 0} |\boldsymbol{c}_{m,n}|^2 \left(k_m^2+k_n^2\right),
$$

where $K_2 \equiv \sqrt{2\beta(1+8/e^2)}$ is obtained by replacing the two integrands with upper bounds from (C 5), and then integrating directly.

Substitute this bound into (C 14) and apply Parseval's theorem again. In view of (C8)–(C10) and the definition $\boldsymbol{c}_{m,n} = (C_u, C_v, C_w)$, what remains can be written in terms of derivatives of the flow. Altogether,

$$
R^{(2)} \leqslant \epsilon h_M K_2 \sqrt{\sum_{(m,n)\neq 0} |\boldsymbol{c}_{m,n}|^2(k_m^2+k_n^2)} = \epsilon h_M K_2 \sqrt{\sum_{(m,n)\neq 0} |ik_m \boldsymbol{c}_{m,n}|^2 + \sum_{(m,n)\neq 0} |ik_n \boldsymbol{c}_{m,n}|^2}
$$

$$
= \epsilon h_M K_2 \sqrt{\left\| \frac{\partial}{\partial x}\left(-h(x,y)\left.\frac{\partial \boldsymbol{u}_1}{\partial z}\right|_{z=0}\right) \right\|_{x,y}^2 + \left\| \frac{\partial}{\partial y}\left(-h(x,y)\left.\frac{\partial \boldsymbol{u}_1}{\partial z}\right|_{z=0}\right) \right\|_{x,y}^2}
$$

$$
= \epsilon h_M K_2 \left\| \nabla\left(h(x,y)\left.\frac{\partial \boldsymbol{u}_1}{\partial z}\right|_{z=0}\right) \right\|_{x,y} = \epsilon h_M K_2 \left\| (\nabla h(x,y))\left.\frac{\partial \boldsymbol{u}_1}{\partial z}\right|_{z=0} + h(x,y) \right.
$$

$$
\left. \times \left(\nabla \left.\frac{\partial \boldsymbol{u}_1}{\partial z}\right|_{z=0}\right) \right\|_{x,y} \leqslant \epsilon h_M K_2 \left(|\nabla h|_M \left\| \left.\frac{\partial \boldsymbol{u}_1}{\partial z}\right|_{z=0}\right\|_{x,y} + h_M \left\| \nabla \left.\frac{\partial \boldsymbol{u}_1}{\partial z}\right|_{z=0}\right\|_{x,y} \right). \tag{C15}
$$

Computing $|\partial\boldsymbol{u}_1/\partial z|^2$ at $z = 0$, the solution takes the form:

$$\left|\frac{\partial\boldsymbol{u}_1}{\partial z}\right|^2_{z=0} = \sum_{j=\{1,2,3\}}\left(\sum_{(m,n)\neq\mathbf{0}}\boldsymbol{\tau}\cdot(\boldsymbol{s}_{m,n}\cdot\boldsymbol{G}_{(j)}\cdot\boldsymbol{t}_{m,n},\ \boldsymbol{s}_{m,n}\cdot\boldsymbol{H}_{(j)}\cdot\boldsymbol{t}_{m,n})\hat{h}(m,n)\mathrm{e}^{\mathrm{i}(k_m x+k_n y)}\right)^2.$$

For

$$\boldsymbol{s}_{m,n} = \left(1,\ \frac{k_m}{\sqrt{k_m^2+k_n^2}},\ \frac{k_n}{\sqrt{k_m^2+k_n^2}}\right)\quad\text{and}\quad\boldsymbol{t}_{m,n} = (k_m, k_n),$$

and $\boldsymbol{G}_{(j)}$ and $\boldsymbol{H}_{(j)}$ constant, dimensionless 3×2 matrices. Parseval's theorem and the Cauchy–Schwarz inequality then give:

$$\left\|\frac{\partial\boldsymbol{u}_1}{\partial z}\right\|^2_{z=0}\bigg|_{x,y} \leqslant \sum_{(m,n)\neq\mathbf{0}}\gamma\ |\boldsymbol{\tau}|^2|\boldsymbol{s}_{m,n}|^2|\boldsymbol{t}_{m,n}|^2|\hat{h}(m,n)|^2$$

$$= 2\gamma\ |\boldsymbol{\tau}|^2\sum_{(m,n)\neq\mathbf{0}}(k_m^2+k_n^2)|\hat{h}(m,n)|^2$$

$$= 2\gamma\ |\boldsymbol{\tau}|^2\left(\left\|\frac{\partial h}{\partial x}\right\|^2_{x,y}+\left\|\frac{\partial h}{\partial y}\right\|^2_{x,y}\right) = 2\gamma\ |\boldsymbol{\tau}|^2\ \|\nabla h\|^2_{x,y}\qquad\text{(C 16)}$$

for

$$\gamma = \sum_{j=\{1,2,3\}}|\boldsymbol{G}_{(j)}|^2+|\boldsymbol{H}_{(j)}|^2.$$

By similar means, we can show

$$\left\|\nabla\frac{\partial\boldsymbol{u}_1}{\partial z}\right\|^2_{z=0} \leqslant \sum_{(m,n)\neq\mathbf{0}}\gamma\ (k_m^2+k_n^2)|\boldsymbol{\tau}|^2|\boldsymbol{s}_{m,n}|^2|\boldsymbol{t}_{m,n}|^2|\hat{h}(m,n)|^2$$

$$= 2\gamma\ |\boldsymbol{\tau}|^2\sum_{(m,n)\neq\mathbf{0}}(k_m^4+k_n^4+2k_m^2 k_n^2)|\hat{h}(m,n)|^2$$

$$= 2\gamma\ |\boldsymbol{\tau}|^2\left(\left\|\frac{\partial^2 h}{\partial x^2}\right\|^2_{x,y}+\left\|\frac{\partial^2 h}{\partial y^2}\right\|^2_{x,y}+2\left\|\frac{\partial^2 h}{\partial x\,\partial y}\right\|^2_{x,y}\right) = 2\gamma\ |\boldsymbol{\tau}|^2\ \|\nabla\nabla h\|^2_{x,y}.$$

$$\text{(C 17)}$$

Applying (C 16) and (C 17) to (C 15), and absorbing $\sqrt{2\gamma}$ into the definition of K_2, we obtain the final result:

$$R^{(2)} \leqslant \epsilon h_M K_2|\boldsymbol{\tau}|(|\nabla h|_M\ \|\nabla h\|_{x,y} + h_M\ \|\nabla\nabla h\|_{x,y}).$$

REFERENCES

AJDARI, A. 2002 Transverse electrokinetic and microfluidic effects in micropatterned channels: lubrication analysis for slab geometries. *Phys. Rev. E* **65** (1), 016301.

BATCHELOR, G. K. 1970 Slender-body theory for particles of arbitary cross-section in Stokes flow. *J. Fluid Mech.* **44**, 419–440.

BAZANT, M. Z. & VINOGRADOVA, O. I. 2008 Tensorial hydrodynamic slip. *J. Fluid Mech.* **613**, 125–134.

BECHERT, D. W. & BARTENWERFER, M. 1989 The viscous flow on surfaces with longitudinal ribs. *J. Fluid Mech.* **206**, 105–129.

BOCQUET, L. & BARRAT, J. L. 2007 Flow boundary conditions from nano- to micro-scales. *Soft Matter* **3**, 685–693.

DAVIS, A. M. J. & LAUGA, E. 2009 Geometric transition in friction for flow over a bubble mattress. *Phys. Fluids* **21**, 011701.

FEUILLEBOIS, F., BAZANT, M. Z. & VINOGRADOVA, O. I. 2009 Effective slip over superhydrophobic surfaces in thin channels. *Phys. Rev. Lett.* **102**, 026001.

HIGDON, J. J. L. 1985 Stokes flow in arbitrary two-dimensional domains: shear flow over ridges and cavities. *J. Fluid Mech.* **159**, 195–226.

HINCH, E. J. 1991 *Perturbation Methods*. Cambridge University Press.

HOCKING, L. M. 1976 A moving fluid interface on a rough surface. *J. Fluid Mech* **76**, 801–817.

JUNG, Y. & TORQUATO, S. 2005 Fluid permeabilities of triply periodic minimal surfaces. *Phys. Rev. E* **72**, 056319.

KUNERT, C. & HARTING, J. 2008 Simulation of fluid flow in hydrophobic rough microchannels. *Intl J. Comput. Fluid D* **27** (7), 475–480.

LAUGA, E., BRENNER, M. P. & STONE, H. A. 2007 *Handbook of Experimental Fluid Dynamics*, Ch. 19, pp. 1219–1240. Springer.

LAUGA, E. & STONE, H. A. 2003 Effective slip in pressure-driven Stokes flow. *J. Fluid Mech.* **489**, 55–77.

LUCHINI, P., MANZO, F. & POZZI, A. 1991 Resistance of a grooved surface to parallel flow and cross-flow. *J. Fluid Mech.* **228**, 87–109.

MIKSIS, M. J. & DAVIS, S. H. 1994 Slip over rough and coated surfaces. *J. Fluid Mech.* **273**, 125–139.

PANZER, P., LIU, M. & EINZEL, D. 1992 The effects of boundary curvature on hydrodynamic fluid flow: calculation of slip lengths. *Intl J. Mod. Phys.* B **6** (20), 3251.

PRIEZJEV, N. V. & TROIAN, S. M. 2006 Influence of periodic wall roughness on the slip behaviour at liquid/solid interfaces: molecular-scale simulations versus continuum predictions. *J. Fluid Mech.* **554**, 25–46.

SARKAR, K. & PROSPERETTI, A. 1996 Effective boundary conditions for Stokes flow over a rough surface. *J. Fluid Mech.* **316**, 223–240.

SBRAGAGLIA, M. & PROSPERETTI, A. 2007 Effective velocity boundary condition at a mixed slip surface. *J. Fluid Mech.* **578**, 435–451.

STONE, H. A., STROOCK, A. D. & AJDARI, A. 2004 Engineering flows in small devices. *Annu. Rev. Fluid Mech.* **36**, 381–411.

STROOCK, A. D., DERTINGER, S. K. W., AJDARI, A., MEZIĆ, I., STONE, H. A. & WHITESIDES, G. M. 2002*a* Chaotic mixer for microchannels. *Science* **295**, 647–651.

STROOCK, A. D., DERTINGER, S. K., WHITESIDES, G. M. & AJDARI, A. 2002*b* Patterning flows using grooved surfaces. *Anal. Chem.* **74**, 5306–5312.

TORQUATO, S. 2002 *Random Heterogeneous Materials*. Springer.

TUCK, E. O. & KOUZOUBOV, A. 1995 A laminar roughness boundary condition. *J. Fluid Mech.* **300**, 59–70.

VINOGRADOVA, O. I. 1999 Slippage of water over hydrophobic surfaces. *Intl J. Miner. Proc.* **56**, 31–60.

WANG, C.-Y. 1978 Drag due to a striated boundary in slow Couette flow. *Phys. Fluids* **21** (4), 697–698.

WANG, C.-Y. 1994 The Stokes drag clue to the sliding of a smooth plate over a finned plate. *Phys. Fluids* **6** (7), 2248–2252.

WANG, C.-Y. 2003 Flow over a surface with parallel grooves. *Phys. Fluids* **15**, 1114–1121.

WANG, C.-Y. 2004 Stokes flow through a channel with three-dimensional bumpy walls. *Phys. Fluids* **16** (6), 2136–2139.

WILKENING, J. 2009 Practical error estimates for Reynolds' lubrication approximation and its higher order corrections. *SIAM J. Math. Anal.* **41**, 588–630.

ZHOU, H., MARTINUZZI, R. J. & STRAATMAN, A. G. 1995 On the validity of the perturbation approach for the flow inside weakly modulated channels. *Intl J. Numer. Methods Fluids* **39**, 1139–1159.